#### **Research Article**

Tanveer Sajid, Salem Algarni, Hijaz Ahmad, Talal Alqahtani, Wasim Jamshed\*, Mohamed R. Eid, Kashif Irshad, and Ayesha Amjad

# Exploration of irreversibility process and thermal energy of a tetra hybrid radiative binary nanofluid focusing on solar implementations

https://doi.org/10.1515/ntrev-2024-0040 received January 13, 2024; accepted May 17, 2024

Abstract: Thermal energy from the Sun comes mostly from sunlight. These energies might be used in photovoltaic cells, sustainable power systems, solar light poles, and water-collecting solar pumps. This age studies solar energy and how direct sunshine might improve solar panel efficiency. Solar energy, especially solar tiles, is widely used in manufacturing today. The literature includes a modified Buongiorno hybrid nanofluid prototype. There are no studies that have examined the impact of tri-hybrid and unique tetra hybridity nanomolecules integrated with the Buongiorno nanofluid prototype on liquid moving on a flexible surface. This study examines the effects of an improved Buongiorno tetra hybrid nanofluid prototypical with Buongiorno and Tiwari–Das nanofluid on magnetized double-diffusive binary nanofluid with cross fluid and

Maxwell liquid flowing with variant thermal conductance over a porous medium. Different profiles include diffusion thermo and thermo diffusion. The LobattoIIIA scheme's convergence and stability are examined in terms of residual error, mesh points for ordinary differential equations (ODEs), and boundary conditions. Leading equations about liquid flow continuity, impetus, temperature, and concentricity are obtained using continuity, conservation of momentum, the second law of thermodynamics, Fick's second law of diffusion, and boundary layer expectations. The system of partial differential equations obtained from the given assumption becomes a system of ODEs and well-established LobattoIII. Their numerical solution is obtained using a numerical technique. Statistical charts and tables provide numerical solutions. The heat transport rate of tetra-hybrid nanomolecules increases dramatically, unlike tri- and di-hybrid nanomolecules. The improved Buongiorno tetra hybrid nanofluid (BTHNF) model produces more heat when radiation Rd, Brownian diffusion Nb, and thermal conductivity are increased. The data show that the diffusion factor L, Brinkman number Br, and Reynolds number Re increase entropy production, but Bejan number reduces it owing to an increase in Be and Re. A statistical regression study shows that retaining the Maxwell fluid parameter constant and increasing the Weissenberg number We decrease the drag coefficient error. A BTHNF model containing tetra hybrid nanoparticles has not been utilized to examine heat and mass transferences in non-Newtonian fluids, considering diffusion, thermo, and thermo diffusion. Entropy generation in a binary fluid with tetra hybrid nanoparticles and BTHNF has not been studied. Tetra hybrid nanofluid is not mentioned in the literature. This effort aims to create a new tetra-hybrid nanofluid model. This article is novel because it investigates the effects of thermal radiation, thermal conductivity, porosity, Darcy-Forchheimer, and Buongiorno models on a tetra-hybrid

**Keywords:** binary fluid, thermal radiation, double diffusion, porosity, tetra hybridity nanofluid, irreversibility, solar implementation

nanofluid flow under an extensible sheet.

\* Corresponding author: Wasim Jamshed, Department of

Hijaz Ahmad: Department of Mathematics, Faculty of Science, Islamic University of Madinah, Madinah, 42351, Saudi Arabia; Near East University, Operational Research Center in Healthcare, TRNC Mersin 10, Nicosia, 99138, Turkey; Center for Applied Mathematics and Bioinformatics, Gulf University for Science and Technology, Mishref, Kuwait; Department of Computer Science and Mathematics, Lebanese American University, Beirut, Lebanon

**Mohamed R. Eid:** Finance and Insurance Department, College of Business Administration, Northern Border University, Arar 1321, Saudi Arabia **Kashif Irshad:** Interdisciplinary Research Centre for Sustainable Energy Systems (IRC-SES), Research Institute, King Fahd University of Petroleum and Minerals (KFUPM), Dhahran, 31261, Saudi Arabia

**Ayesha Amjad:** Faculty of Organisation and Management, Silesian university of Technology Gliwice, 44-100, Poland

Mathematics, Capital University of Science and Technology (CUST), Islamabad, 44000, Pakistan; Mathematics in Applied Sciences and Engineering Research Group, Scientific Research Center, Al-Ayen University, Nasiriyah, 64001, Iraq, e-mail: wasiktk@hotmail.com Tanveer Sajid: Department of Mathematics, Capital University of Science and Technology (CUST), Islamabad, 44000, Pakistan Salem Algarni, Talal Alqahtani: Mechanical Engineering Department, College of Engineering, King Khalid University, Abha, 9004, Saudi Arabia Hijaz Ahmad: Department of Mathematics, Faculty of Science, Islamic University of Madinah, Madinah, 42351, Saudi Arabia; Near Fact

2 — Tanveer Sajid et al. DE GRUYTER

#### **Abbreviations**

AC alternating current

BTHNF Buongiorno tetra hybrid nanofluid C-CHF Cattaneo-Christov heat fluxing

DC direct current
HNF hybrid nanofluid
LFRs linear Fresnel mirrors

MBNF modified Buongiorno nanofluid

MHD magneto hydrodynamics

PV photovoltaic

THNF tetra hybrid nanofluid

#### 1 Introduction

Due to intricate stress-strain relationships, non-Newtonian fluids are hard to predict. This Maxwell-cross model, which combines viscoelastic and power law models, can simulate flow in the power law zone and regions with low and high shear rates. This model also accurately describes territory movement at low and high shear rates and liquid relaxation time. This technique requires temporal relaxation but can conduct many scientific simulations. Everyday Maxwell-cross fluids include tomato sauce, paint, and blood. Megahed and Abbas [1] studied stratified cross-fluid flow, porosity material, and chemical reactions and found that porosity limitation increases the slow fluid flow. This shows that chemical reactions have a significant impact. Hauswirth and colleagues [2] found that porosity reduced the velocity when the cross model traveled over an expanding sheet by increasing the Weissenberg quantity. Patel [3] showed that when a magnetic force acts on stalled Carreau liquid in a porous medium, the liquid temperature increases with the heat production factor. Research investigating magnetic effects on Carreau liquid revealed this. Shaw et al. [4] and Sahu et al. [5] found that nonlinearly based thermal radiative fluxing transfers heat faster than thermal radiation in a cross-liquid. They also observed that the Darcy-Forchheimer effect amplification lowered the liquid flow speed. An implanted cross-nanofluid with a Cattaneo-Christov heat fluxing (C-CHF) and chemical reaction was thoroughly studied by Ramzan et al. [6]. They found that C-CHF increases heat transfer. The heat transfer study of a cross-nanoliquid via a parabolic trough surface collector was extensively studied by Reddy et al. [7]. Chemical reactions and MHD effects on crossflow liquid in an inflatable cylinder were examined by Ali et al. [8]. They observed that magnetized force improvement reduced the speed field. Azam et al. [9] examined how

sun radiation affects unsteady cross-nanoliquid. They found that sunlight raises the fluid temperature.

Recent studies have examined triple HNF effects on fluid dynamics and thermal convection. In energy connections, triple hybrid nanocomposites surpass regular liquids, nanofluid, mixed nanofluid, petroleum, and ethanol. We cannot compare them with regular liquids. Hybrid nanofluids may freeze under hot conditions and other temperature-dependent phenomena. Recent research has examined the impact of ternary hybrid nanofluids on fluid flow in complex geometries. Asghar et al. [10] analyzed how HNF affected a fluid flow under the sheet that was expanding and contracting with the inclusion of thermal radiation and rotating effect. While studying the effects of tri-hybrid nanoparticles and thermal radiative consequence on a waterbased nanoliquid passing a rotative sphere, Khan et al. [11] discovered that a boost in thermal radiation increases the Nusselt number. Heat transfer is amplified because of enlargement in the fractional size of ternary hybridity nanomolecules, as reported by Algehyne et al. [12], who assessed the impact of tri-nanomolecules on pseudoplastic liquid movement exposed toward a porousness material. The effect of copper-alumina/water-based nanoliquid with the inclusion of the magnetic effect and slip condition was probed by Rasool et al. [13]. Hou et al. [14] examined the Soret/Dufour type influence on pseudoplastic THNF and found that even amplification inhibits mass transmission. Praksha et al. [15] compared the di- and tri-hybrid nanofluid flow subjected to an expanding sheet and showed that THNF magnifies the Nusselt number. Sarada et al. [16] found that the heat-generating factor increases the THNF interior temperature. Shamshuddin et al. [17] examined how linear-based thermal rays and the Hall current affect THNF flow toward a rotating disk. Using a wedge, Sajid et al. [18] explained how chemical processes and activation affect THNF. Rosca et al. [19] used a modified Buongiorno nanofluid model (MBNF) on fluid in an elastic media with zero mass flux. Puneeth et al. [20] examined how microorganisms and thermal conductivity affected modified Buongiorno ternary hybrid nanofluid flow toward expandable media and found that the THNF volume percentage greatly increases the heat phenomenon. MBNF flow into a bi-directional stretching medium was examined by Owhaib and Al-Kouj [21]. Ramesh et al. [22] observed MBNF flow via a thin needle and found that the ternary hybrid nanofluid temperature increased more than the hybrid liquid. Ali et al. [23] employed FEM for unsteady rotational flow utilizing MBNF and found that growing an unsteady parameter debacles the liquid velocity. Rana and Gupta [24] solved a three-dimensional fluid embedded with MBNF traveling over an expanding sheet with zero mass flux using a finite element technique. Rana et al. [25]

examined the buoyancy impact on fluid embedded with MBNF across a slippery plate and found that the liquid speed decreases. Sabu et al. examined magneto hybridity nanoliquid flowing over slippery, porous material using MBNF [26]. Alblawi et al. [27] examined exponentially curved MBNF flow.

The Soret and Dufour effects in fluid mechanics and heat transfer explain non-uniform mass and energy transport in fluid mixtures. These effects are especially important in multicomponent mixes with temperature and concentration gradients. Researchers worldwide have studied the effects of diffusion thermo and thermo diffusion on the fluid flow over an expanding sheet. Cross-diffusion and double-diffusion convection in a Casson liquid flow on the Riga plate were studied by Asogwa et al. [28]. Shoaib et al. [29] examined Soret and Dufour's effects on tilted nanofluid flow. Yadav et al. [30] examined Soret and Dufour-type phenomena on fluid flow via a porous expandable sheet. Ramchandraiah et al. [31] examined Soret and Dufour's effects on bidispersive medium. Murray and Chen [32] studied thermal and diffusion processes on flow in a porous elastic media. Asghar et al. [33] studied mixed convection on heat-generating/absorbing hybrid nanoliquid. Yogeesha et al. [34] studied Stefan blowing and the Soret/ Dufour effect on a ternary hybrid nanofluid fluid exposed to a porous, unsteady expanding sheet and found that the Dufour effect increases the fluid temperature. Hafeez et al. [35] considered the Soret/Dufour impact on a hybrid Casson nanoliquid with ethylene glycol. Song et al. [36] discussed hybrid nanofluid non-linear heat generation (sinking).

The amount of entropy created by irreversible processes in a thermodynamic system is called "entropy generation." This definition of "processes" includes heat transmission via a liquid, viscosity, diffusion, heat flux, dispersion, permeability, and more. According to the second principle of thermodynamics, an increase in total entropy during a process that may be interrupted and restarted is undesirable. Nanofluid commonly suffers irreversible events such as dispersion, viscosity-induced fluid friction, heat flux, permeability, and others while traveling over that medium, which might increase the structure's total entropy. Even nanofluid travels through these and other phenomena. Minimizing a system's power sources requires entropy production. The researchers aim to lower entropy from a number of industrial processes and situations. The objective is to increase productivity and output. Dharmaiah et al. [37] investigated the influence of thermal radiation on the tangent hyperbolic nanofluid as it moved over the cone, while mixed convection and activation energy were also considered. Nasir et al. [38] explored the influence of nanoparticles on the Maxwell nanoliquid as it moved toward an exponential wall. Throughout their research, they also achieved the irreversibility of liquid

flow. Berrehal et al. [39] studied entropy generation analysis of hybrid nanofluid flow subjected to a thermic moving wedge. They discovered that the total entropy of the system increases as a result of expansion, as in the Brinkman quantity. Oweidi et al. [40] investigated in depth the entropy generation of ternary hybrid nanofluids traveling through such a rotating disc supplemented with Hall current and also thermal radiation. Naz et al. [41] recalculated the entropy production of magnetized Cross-nano liquid across an elastomeric sheet consisting of motile microbes. Dharmaiah et al. [42] evaluated the effect that a magnetic field combined with activation had on a Buongiorno nanofluid flow toward Howarth's wavy cylinder.

Regression characterization typically uses mathematical formulae. However, differential equations (DEs) may be beneficial for certain modeling situations. Creating a DE model for data collection and then making informed assumptions about the model's uncertain variable quantities based on those estimates and values may achieve this. Quadratic regression (QRE) is used to obtain the best-fitting parabola regression equation for data collection. This extrapolation is an extension of linear regression, which was used to create a straight-line equation that fits the data. One kind of regression calculates the equation of a straight line that best explains a set of data. To solve model-based DEs linked to liquid flow across stretchy media faster, researchers worldwide have been employing regression analysis to examine the relationship between two parameters. Falodun and Ige [43] analyzed the Casson-Williamson nanofluid using linear and quadratic regression and control the chemical processes and heat radiation. Sajid et al. [44] performed a quadratic regression analysis of a Reiner-Philippoff fluid with a heat source, sink, and hybrid nanofluid and used Galerkin finite-element method to calculate the model's numerical findings. Nandi et al. [45] performed a QRE analysis of a stationary hybrid nanofluid in an exponentially expanding medium with a magnetic field and radiation heat effect. A magnetically inclined Carreau nanoliquid was numerically calculated by El-Din et al. [46] using spectrum relaxation. They used QRE regression to study the dynamics of attained dimensional measurements to better understand their behavior. Raju et al. [47] studied a thermally radiated axisymmetric ternary hybrid nanofluid flow toward expanding and contracting permeable barriers using simple linear regression.

With regard to the above-stated literature, the objective of this examination is to inspect the impression of the intended novel modified tetra hybridized Buongiorno nanoliquid model on Maxwell-cross nanofluid in the presence of Soret/Dufour, thermal conductance, and thermal radiative effects. A Maxwell-cross fluid with these types of effects,

especially by consumption of a transformed Buongiorno tetra hybrid nanoliquid simulation, has not been discovered yet in the existing literature. Entropy generation and quadratic regression analysis of a tetra hybrid liquid is not available in the literature.

observed at night. This energy pertains to the use of power inside residential buildings, gardens, outdoor spaces, garages, and security lighting systems.

**DE GRUYTER** 

#### 2 Mechanism of solar-powered tiles

#### 2.1 Solar tiles

Solar radiation is a very potent technique for harnessing solar energy. Solar energy emitted by the Sun immediately reaches photovoltaic cells located on the surface of the solar tiles. A nanofluid containing tetra-hybridized nanomolecules flows across a stretched sheet positioned underneath the PV cells sheet inside the solar tiles. A tetra-hybridized nanofluid is being directed across a plate that is being stretched. Solar radiation passes through the PV solar panel sheet and is incident on the stretched surface. The addition of tetra-hybrid nanomolecules significantly enhances the solar panels' ability to absorb solar energy. More heating is absorbed by the panel because of tetra hybrid nanoparticles present inside the solar panel sheet.

#### 2.2 Power controller

A solar-powered charge controller protects the battery from being overcharged by regulating both the voltage and the current that goes from the solar panel to the battery. This keeps the battery from being in an unstable state. With maximum power point tracking technology, the solar panel can charge the battery 30% quicker each day. The setting for this technology is 15 A/200 W.

#### 2.3 Batteries packed with equipment

Solar tiles employ solar energy to generate electricity, storing the power in their built-in batteries for future use instead of relying on fuel. A pack of batteries is a device that stores energy for later use. The photovoltaic technology harnesses solar energy to generate electricity, which is then stored in a battery. The longer the electrical system in houses gets charged throughout daytime hours when it is exposed to sunshine, the fewer issues will be

#### 2.4 Solar inverter

Among the many crucial components of a solar power setup is an inverter, which is a machine that converts the DC power a solar array generates into AC power that even the power company's power lines require. Multitasking is likely built into a converter in a residential solar power system. It may also serve as a hub for connecting to other networks and monitoring the system while turning solar energy into AC electricity. The ability of solar-based devices, in addition to battery storage devices, to continue functioning in the absence of grid assistance during outages is dependent on the use of sophisticated inverters (Figure 1).

#### 3 Problem formulation

Two-dimensional incompressible laminar binary fluid (cross fluid + Maxwell fluid) is moving subjected to an expandable surface having an extending rate  $u_w = ax$ , where a > 0, in this case, represents the rate at which the sheet is expanding. The stretching sheet over which the tetra hybrid is flowing is located below the PV sheet of the solar tiles sheet, as shown in Figure 2. Porous media is contemplated to probe the outcome of fluid moving through the pores in the light of Darcy law and permeability of the medium. A modified nanofluid model combining the Buongiorno nanofluid and Tiwari-Das model comprising agglomerative tetra nanoparticles (Zn + TiO<sub>2</sub> + Ag + Al<sub>2</sub>O<sub>3</sub>) with EG as a base fluid is considered to investigate the impact of the nanoparticles on a fluid flow. Soret effects are considered for the investigation of the impact of concentration on temperature and the impact of temperature on concentration. Analysis of irreversibility in terms of a fluid flow is evaluated. T,  $T_{\rm w}$ , and  $T_{\infty}$  represent temperatures at the surface in addition to ambient temperature, and C,  $C_{\rm w}$ , and  $C_{\infty}$  represent concentrations at the surface in addition to ambient, respectively.  $\Gamma$ , n, Fr,  $\lambda$ ,  $D_{\text{TC}}$ ,  $D_{\text{CT}}$ ,  $\rho_{\text{tethnf}}$ ,  $\mu_{\text{tethnf}}$ ,  $(\rho C_p)_{\text{tethnf}}$ , and  $k_{\text{tethnf}}$  represent the Maxwell fluid relaxation time, power law index of fluid, Forchheimer term, porosity, diffusion thermo, and thermo diffusion, the density of tetra nanofluid, dynamic viscosity, specific heat, and thermal conductance of a tetra hybridized nanoliquid. The law of conservation of momentum, the second law of thermodynamics,

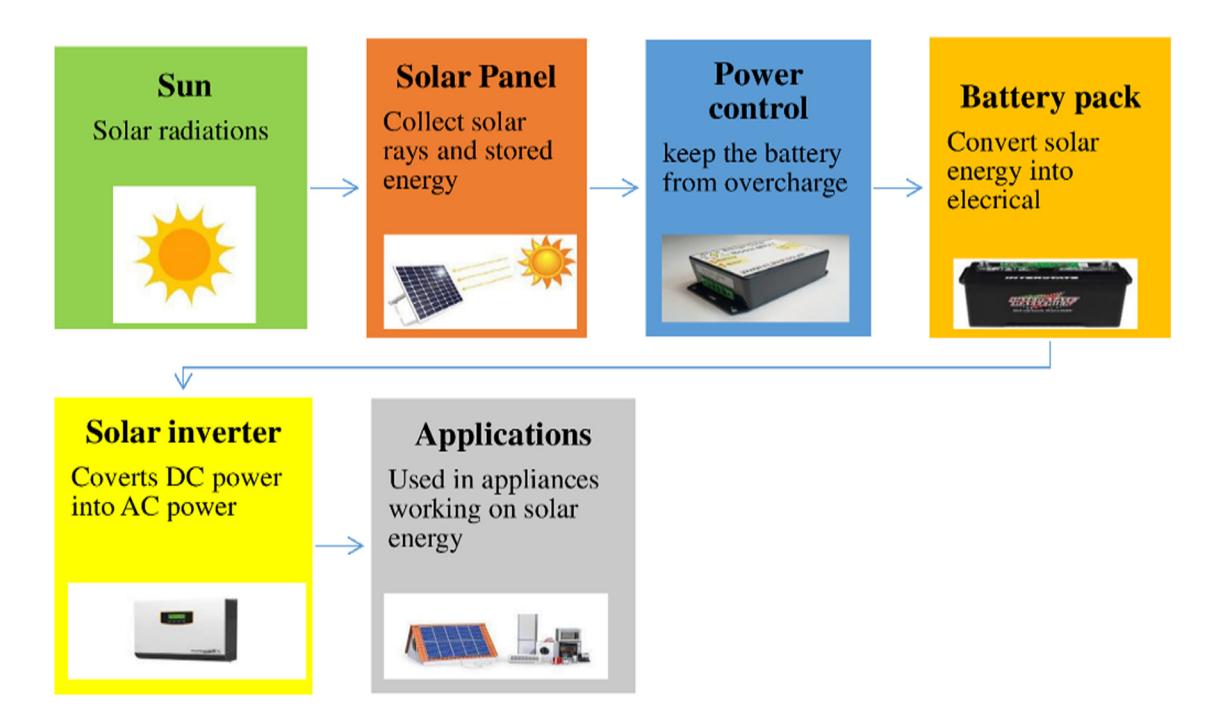


Figure 1: Mechanism of solar comprising of solar tiles.

and Fick's second law in terms of diffusions are utilized in order to obtain equations (2)-(4). The modeled system of equations under the application of boundary layer theory and the above-mentioned assumptions are as follows [24,30,31]:

$$\frac{\partial u}{\partial x} + \frac{\partial v}{\partial y} = 0, (1)$$

$$u\frac{\partial u}{\partial x} + v\frac{\partial u}{\partial y} + \lambda_{1} \left[ u^{2} \frac{\partial^{2} u}{\partial x^{2}} + v^{2} \frac{\partial^{2} u}{\partial y^{2}} + 2uv \frac{\partial^{2} u}{\partial x \partial y} \right]$$

$$= \frac{\mu_{\text{tetnf}}}{\rho_{\text{tetnf}}} \frac{\partial}{\partial y} \left[ \frac{\frac{\partial u}{\partial y}}{1 + \left[ \Gamma \left( \frac{\partial u}{\partial y} \right) \right]^{n}} \right] - \frac{v_{\text{tetnf}}}{K_{1}} u - \frac{1}{\rho_{\text{tetnf}}} Fu^{2},$$
(2)

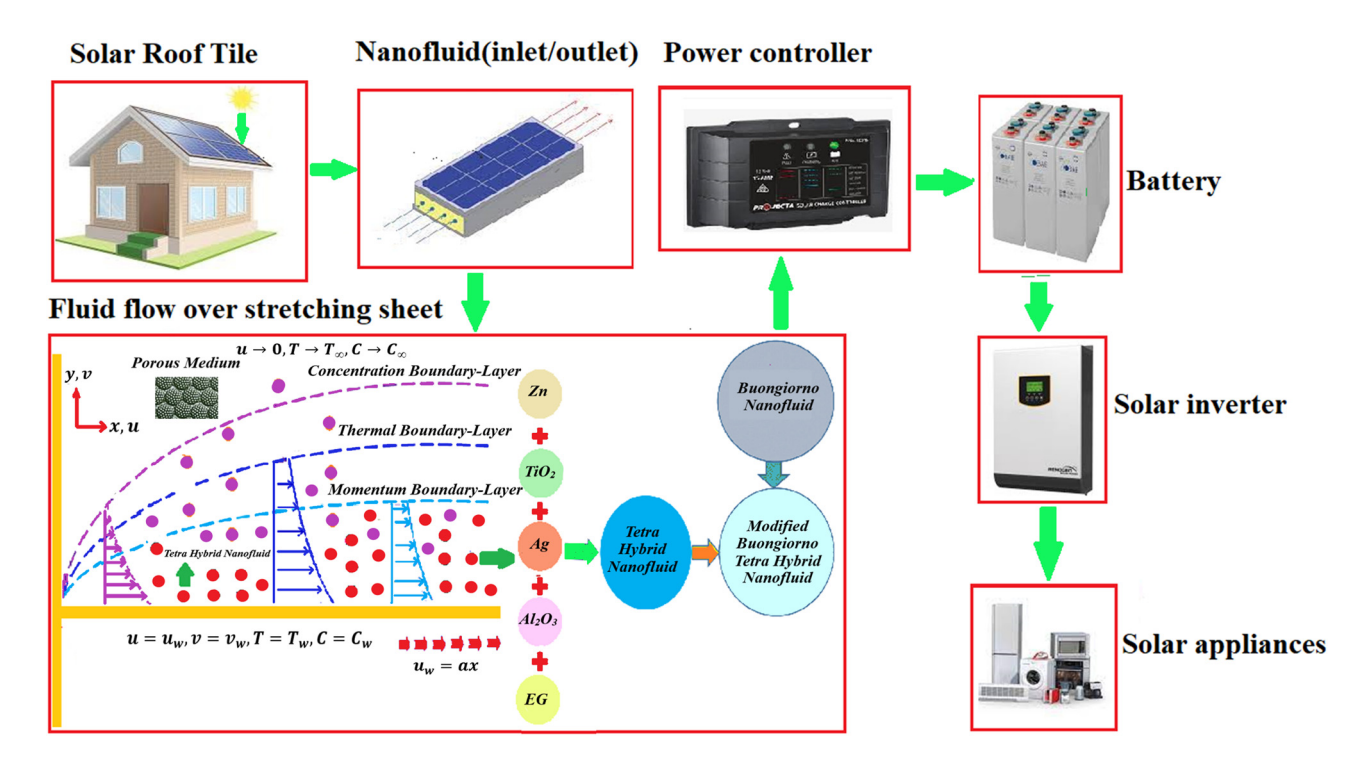


Figure 2: Flow behavior.

(4)

$$\left(u\frac{\partial}{\partial x} + v\frac{\partial}{\partial y}\right)T = \frac{1}{(\rho c_{\rm p})_{\rm tetnf}} \left\{\frac{\partial}{\partial y} \left[k_{\rm tetnf}(T)\right] \frac{\partial T}{\partial y}\right\} 
+ \tau \left[D_{\rm B} \frac{\partial C}{\partial y} \frac{\partial T}{\partial y} + \frac{D_{\rm T}}{T_{\infty}} \left(\frac{\partial T}{\partial y}\right)^{2}\right] 
+ \frac{D_{\rm B} K_{\rm T}}{c_{\rm p} c_{\rm s}} \frac{\partial^{2} C}{\partial y^{2}} - \frac{1}{(\rho c_{\rm p})_{\rm tetnf}} \frac{\partial q_{\rm r}}{\partial y},$$
(3)

$$\left(u\frac{\partial}{\partial x} + v\frac{\partial}{\partial y}\right)C = D_{\rm B}\frac{\partial^2 C}{\partial y^2} + \frac{D_{\rm T}}{T_{\infty}}\frac{\partial^2 T}{\partial y^2} + D_{\rm CT}\frac{\partial^2 T}{\partial y^2},$$

with boundary conditions

$$u = u_{w}x, v = v_{w}, T = T_{w}, C = C_{w} \text{ at } y = 0,$$

$$u \to 0, T \to T_{\infty}, C \to C_{\infty} \text{ as } y \to \infty.$$

Temperature-based heat conduction is

$$k_{\text{tetnf}}(T) = k_{\text{tetnf}} \left[ 1 + \varepsilon \left( \frac{T - T_{\infty}}{T_{w} - T_{\infty}} \right) \right],$$
 (6)

whereas

$$\mu_{\text{tethnf}} = \frac{\mu_{\text{f}}}{(1 - \phi_{1})^{2.5}(1 - \phi_{2})^{2.5}(1 - \phi_{3})^{2.5}(1 - \phi_{4})^{2.5}},$$

$$\rho_{\text{tethnf}} = [(1 - \phi_{4})\{(1 - \phi_{3})(1 - \phi_{2})[(1 - \phi_{1})\phi_{f} + \rho_{1}\phi_{1}] + \rho_{2}\phi_{2} + \rho_{3}3\} + \rho_{4}\phi_{4}],$$

$$(\rho C_{\text{p}})_{\text{tethnf}} = (1 - \phi_{4})\{(1 - \phi_{3})(1 - \phi_{2})[(1 - \phi_{1})(\rho C_{\text{p}})_{f} + (\rho C_{\text{p}})_{s_{1}}\phi_{1}] + (\rho C_{\text{p}})_{s_{2}}\phi_{2} + (\rho C_{\text{p}})_{s_{3}}\phi_{3}\} + (\rho C_{\text{p}})_{s_{4}}\phi_{4},$$

$$\frac{k_{\text{tethnf}}}{k_{\text{f}}} = \frac{k_{4} + 2k_{\text{thnf}} - 2\phi_{4}(k_{\text{thnf}} - k_{4})}{k_{4} + 2k_{\text{thnf}} + \phi_{4}(k_{\text{thnf}} - k_{4})},$$

$$\frac{k_{\text{thnf}}}{k_{\text{f}}} = \frac{k_{3} + 2k_{\text{hnf}} - 2\phi_{3}(k_{\text{hnf}} - k_{3})}{k_{3} + 2k_{\text{hnf}} + \phi_{3}(k_{\text{hnf}} - k_{3})},$$

$$\frac{k_{\text{hnf}}}{k_{\text{f}}} = \frac{k_{2} + 2k_{\text{nf}} - 2\phi_{2}(k_{\text{nf}} - k_{2})}{k_{2} + 2k_{\text{nf}} + \phi_{2}(k_{\text{nf}} - k_{2})},$$

$$\frac{k_{\text{nf}}}{k_{\text{f}}} = \frac{k_{1} + 2k_{\text{f}} - 2\phi_{1}(k_{\text{f}} - k_{1})}{k_{1} + 2k_{\text{f}} + \phi_{1}(k_{\text{f}} - k_{1})}.$$

$$(7)$$

The symbols  $\phi_1$ ,  $\phi_2$ ,  $\phi_3$ ,  $\phi_4$ ,  $\mu_{\text{tethnf}}$ ,  $\rho_{\text{tethnf}}$ ,  $k_{\text{tethnf}}$ ,  $(\rho C_p)_{\text{tethnf}}, k_{\text{thnf}}, k_{\text{nf}}, k_{\text{f}}, \text{ and } (\rho C_p)_{\text{f}}$  represent the fractional size of nanoparticles  $(\phi_1, \phi_2, \phi_3, \phi_4)$ , where  $\phi = \phi_1 + \phi_2$  $\phi_2$  +  $\phi_3$  +  $\phi_4$  in the range of 0.01–0.1. Zinc (Zn) and their Zn oxide nanoparticles have excellent chemical, electrical, and thermal stability. Zinc oxide nanoparticles also have optical, electrical, and photocatalytic properties. Alumina (Al<sub>2</sub>O<sub>3</sub>) nanoparticles are valued for their enhanced properties compared to bulk materials. These particles, less than 100 nm in diameter, exhibit improved hardness, strength, and conductivity due to their small size. Silver (Ag) nanoparticles have been proven to exhibit excellent electrical conductivity, chemical stability, and catalytic and antimicrobial properties. The lightweight, high strength, and external corrosion resistance of titanium and its alloys (TiO2) enables them to be used in the aviation industry. Titanium alloys have an excellent strength-to-weight ratio.

The thermophysical properties of Zn,  $TiO_2$ , Ag, and  $Al_2O_3$ , along with the base fluid EG [16,18,44,48–50], are displayed in Table 1.

Adopting similarity variables [24,30,31],

$$\eta = \sqrt{\frac{a}{v}y}, \psi = \sqrt{av}xf(\eta), \theta = \frac{T - T_{\infty}}{T_{w} - T_{\infty}}, \varphi = \frac{C - C_{\infty}}{C_{w} - C_{\infty}}.$$
 (8)

After transformations, equations (2)–(4) together with (5) are as follows:

$$[(1 - (n - 1)(Wef'')^n)]f''' + A_1A_2(1 + (Wef'')^n)^2(ff'' - f'^2 - Frf'^2) - \Lambda A_1A_2(f^2f''' - 2ff'f'') - \lambda f' = 0,$$
(9)

(5) 
$$\left[ (1 + \varepsilon \theta) + \frac{4}{3A_4} \operatorname{Rd} \right] \theta'' + \varepsilon \theta'^2 + A_4 \operatorname{Pr}(\operatorname{Nb} \theta' \varphi' + \operatorname{Nt} \theta'^2) + A_3 \operatorname{Pr}(Df'' + f\theta') = 0,$$
 (10)

$$\varphi'' + \frac{Nt}{Nh}\theta'' + Scf\varphi' + ScSr'' = 0, \tag{11}$$

$$f'(\eta) = 1, f(\eta) = 0, \theta(\eta) = 1, \text{ at } \eta = 0,$$
  
$$f'(\eta) \to 0, \theta(\eta) \to 0, \varphi(\eta) \to 0, \text{ as } \eta \to \infty.$$
 (12)

Expressions regarding frictional factors in additional heat transference rate are

$$Cf = \frac{2\tau_{w}}{\rho_{f}u_{w}^{2}}, \quad Nu_{x} = \frac{xq_{w}}{k_{f}(T_{w} - T_{\infty})}.$$
 (13)

The shear stresses  $au_{xy}$  in addition to heat flux at the wall  $q_w$  are premeditated by

$$\tau_{\rm w} = \mu_{\rm tethnf} \left\{ \frac{\partial u}{\partial y} \left[ \frac{1}{1 + \left[ \Gamma \frac{\partial u}{\partial y} \right]^n} \right] + (1 + \Lambda) \frac{\partial u}{\partial y} \right\},$$

$$q_{\rm w} = -k_{\rm tethnf} \frac{\partial T}{\partial y}.$$
(14)

The dimensionless drag coefficient is represented by

Cf Re<sub>x</sub><sup>1/2</sup> = 
$$\frac{1}{A_1} \left( \frac{f''}{1 + (Wef'')^n} + (1 + \Lambda)f'' \right)$$
. (15)

The heat transfer dimensionless form is

**Table 1:** Thermophysical properties of the conventional liquid and solid nanomaterials

Property	EG	Zn	TiO <sub>2</sub>	Ag	Al <sub>2</sub> O <sub>3</sub>
ρ	1113.5	7,140	4,250	10,500	3,970
$C_{\rm p}$	2,430	390	690	235	765
k	0.253	116	8.953	429	40

$$Nu_x Re_x^{-1/2} = -A_4 \theta'$$
 (16)

whereas  $A_1$ ,  $A_2$ ,  $A_3$ , and  $A_4$  are given by

$$A_{1} = \frac{1}{(1 - \phi_{1})^{2.5}(1 - \phi_{2})^{2.5}(1 - \phi_{3})^{2.5}(1 - \phi_{4})^{2.5}},$$

$$A_{2} = (1 - \phi_{1})\left\{(1 - \phi_{2})(1 - \phi_{3})\left[(1 - \phi_{4}) + \phi_{4}\frac{\rho_{4}}{\phi_{f}}\right]\right\}$$

$$+ \phi_{3}\frac{\rho_{3}}{\phi_{f}} + \phi_{2}\frac{\rho_{2}}{\phi_{f}}\right\} + \phi_{1}\frac{\rho_{1}}{\phi_{f}},$$

$$A_{3} = (1 - \phi_{1})\left\{(1 - \phi_{2})(1 - \phi_{3})\left\{(1 - \phi_{4})\right\}\right\}$$

$$+ \frac{(\rho C_{p})_{s_{4}}}{(\rho C_{p})_{f}}\phi_{4}\right\} + \frac{(\rho C_{p})_{s_{3}}}{(\rho C_{p})_{f}}\phi_{3} + \frac{(\rho C_{p})_{s_{2}}}{(\rho C_{p})_{f}}\phi_{2}\right\}$$

$$+ \frac{(\rho C_{p})_{s_{1}}}{(\rho C_{p})_{f}}\phi_{1},$$

$$A_{4} = \frac{k_{\text{tethnf}}}{k_{f}}.$$

The dimensionless parameters in the above equations are presented in Table 2.

#### 4 Entropy generation analysis

The entropy in its mathematical form is given as follows:

$$S_{g} = \frac{k_{f}}{T_{\infty}^{2}} \left[ \frac{k_{\text{tethnf}}}{k_{f}} + \frac{16\sigma^{*}}{3k^{*}k_{f}} \left( \frac{\partial T}{\partial y} \right)^{2} \right]$$

$$+ \frac{\mu_{\text{tethnf}}}{T_{\infty}} \left( \frac{\partial u}{\partial y} \right)^{2} \left[ \frac{1}{1 + \left[ \Gamma \frac{\partial u}{\partial y} \right]^{n}} \right] + \frac{\mu_{\text{tethnf}}}{K} u^{2}$$

$$+ \left( \frac{Rd}{C_{\infty}} \left( \frac{\partial C}{\partial y} \right)^{2} + \frac{Rd}{T_{\infty}} \left( \frac{\partial C}{\partial y} \right) \left( \frac{\partial T}{\partial y} \right) \right)$$

$$(18)$$

unsustainability of concentration. The interpretation in terms of entropy dissipation is

$$N_{\rm g} = \frac{S_{\rm g}}{k_{\rm f}/x^2 \Omega_{\rm T}^2},\tag{19}$$

and the non-dimensional expression of the entropy rate is given by

$$N_{\rm g} = N_{\rm gh} + N_{\rm gf} + N_{\rm gp} + N_{\rm gc}.$$
 (20)

Here,  $N_{\rm gh}$ ,  $N_{\rm gf}$ ,  $N_{\rm gp}$ , and  $N_{\rm gc}$  represent the formation of entropy owing to heat unsustainability, fluid friction unsustainability, porosity irreversibility, and concentration unsustainability, respectively. This concept is quantitatively represented as follows:

$$N_{\rm gh} = (A_4 + \text{Rd})\theta'^2, N_{\rm gf} = \left(\frac{\text{Br}}{A_1\Omega_T}\right)\left[1 + \frac{1}{(\text{We}f'')^n}\right]f''^2,$$

$$N_{\rm gp} = \left(\frac{\text{Br}}{\Omega_T}\right)\frac{k}{A_1}kf'^2, \quad N_{\rm gc} = G\theta'\varphi' + \frac{G\Omega_C}{\Omega_T}\varphi'^2,$$
(21)

although

$$Br = \frac{\mu_{\rm f} u_{\rm e}^2}{k_{\rm f} (T_{\rm w} - T_{\infty})}, \qquad Re_{\rm x} = \frac{u_{\rm e} x}{v_{\rm f}},$$

$$\Omega_{\rm T} = \frac{(T_{\rm w} - T_{\infty})}{T_{\infty}}, \quad \Omega_{\rm C} = \frac{(C_{\rm w} - C_{\infty})}{C_{\infty}}$$
(22)

The formula for calculating the Bejan number is as follows:

Be = 
$$\frac{\text{Heat transfer irreversibilty}}{\text{Total entropy}}$$
, (23)

Be = 
$$\frac{(A_4 + Rd)\theta'^2}{\Omega_T(A_4 + Rd) + \left(\frac{Br}{A_1\Omega_T}\right)\left(1 + \frac{1}{(Wef'')^n}\right)f''^2 + \left(\frac{Br}{\Omega_T}\right)\frac{k}{A_1}kf'^2 + G\theta'\varphi' + \frac{G\Omega_C}{\Omega_T}\varphi'^2}.$$
 (24)

Here, the first term describes the unsustainability of the heat occurrence, the second describes the irreversibility of the liquid friction that is associated with the cross-liquid, the third term describes the irreversibility of a permeability occurrence, and the final term describes the

#### 5 Methodology

Utilizing MATLAB's developed bvp4c code in combination with the LobattoIIIA methodology allows for the dimensionless equation system to be managed numerically. This is

Table 2: Dimensionless parameters [4,5,9,20,29,38]

Dimensionless parameters	Dimensional parameters	Dimensional parameters	
$M^2 = \frac{\sigma B_0^2}{\rho a}$ = magnetic effect	n = power index	Γ = material constant	
$Pr = \frac{\mu c_p}{K^*} = Prandtl number$	$D_{\mathrm{TC}}$ = Dufour type diffusion	g = gravity phenomenon	
$\lambda = \frac{c}{aK} = \text{porosity}$	$D_{\rm CT}$ = Soret type diffusion	$\omega$ = inclination angle	
$Df = \frac{D_{TC}(C_W \ C_{\infty})}{\nu(T_W \ T_{\infty})} = Dufour \ effect$	$D_{\rm SM}$ = concentration diffusion	$K_1$ = porosity	
$Le = \frac{v}{D_{SM}} = Lewis parameter$	S = suction	$\gamma$ = thermal expansion	
$Sr = \frac{D_{CT}(T_W T_{\infty})}{D_{SM}(C_W C_{\infty})} = Soret effect$	$C_{\rm p}$ = heat capacity	$\mu$ = dynamic viscosity	
$\lambda^* = \frac{g\beta_{\rm f}(T_2 T_m)}{u_{\rm w}^2} = \text{convection}$	$\sigma$ = electrical conductivity	ho = density	
$S = \frac{v_{\rm w}}{\sqrt{av}}$ = suction in a fluid	K(T) = thermal conductivity	$B_0$ = magnetic parameter	
$\Lambda = \lambda_1 a$ = Maxwell parameter			

made possible by the LobattoIIIA strategy [51–53]. Throughout this process, the nonlinearly modeled partial differential equations (PDEs), which take into account a variety of effects in momentum energy and concentration formulas, are transferred into ordinary differential equations (ODEs) with the assistance of similarity components. As in the second phase, these ODEs were diminished to first-order ODEs again for the LobattoIIIA methodology by adopting the values  $f=y_1$ ,  $\theta=y_4$ , and  $\phi=y_6$ . The non-dimensional elements were formed throughout the simulation analysis. The rate of surface drag and the amount of heat delivery are both estimated with a number of non-dimensional factors, and the findings are presented in the form of tables and charts. The amount of tolerance that should be applied to this specific case of the problem is  $10^{-6}$ , and in fact, the range of computation should be

[0,7] rather than  $[0, \infty]$ . The process diagram technique of the recommended computation structure is shown in Figure 3:

$$f'=y_2, \quad f''=y_3,$$

$$f''' = y_3'$$

$$= \frac{A_1 A_2 [1 + (Wey_3)^n]^2 [(A_3 M y_2 + Fr y_2^2 + y_2^2 - y_1 y_3] + \lambda y_2 + A_1 A_2 \Lambda (y_1 y_2 y_3)}{(1 + (1 - n)(Wey_3)^n) - \Lambda y_1^2}$$

$$\theta = y_4$$
,  $\theta' = y_5$ ,

$$\theta' = y_5' = y_5' = \frac{-(A_4 \Pr(Nby_5 y_7 + Nty_5^2) + A_4 \Pr(Ndy_7' + y_1 y_5) - \varepsilon y_5^2)}{\left((1 + \varepsilon y_4) + \frac{4}{3A_5} Rd\right)},$$

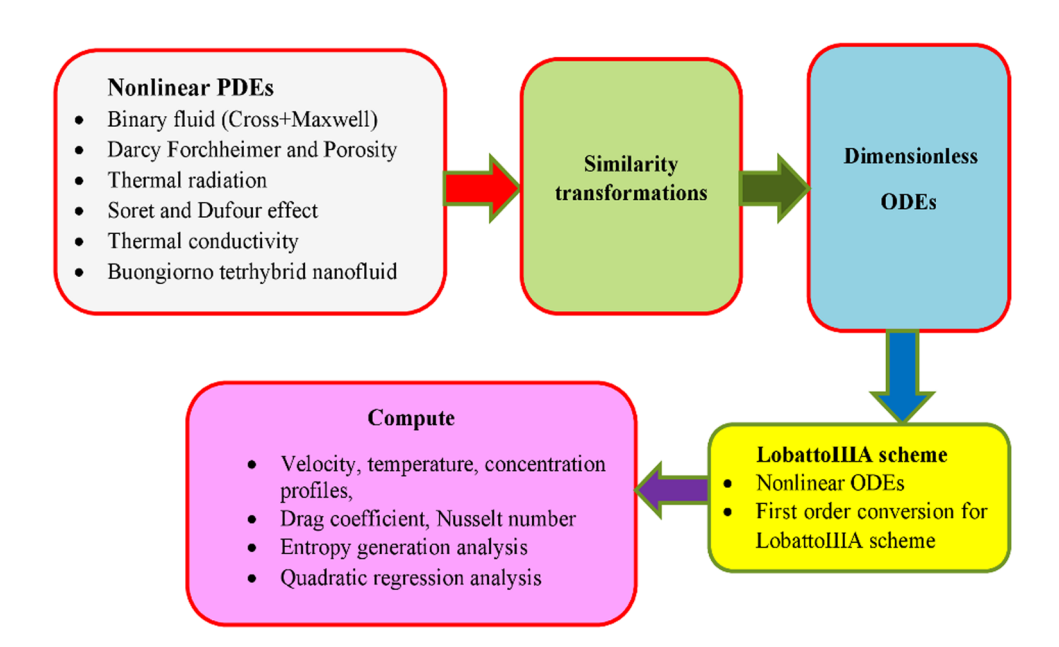
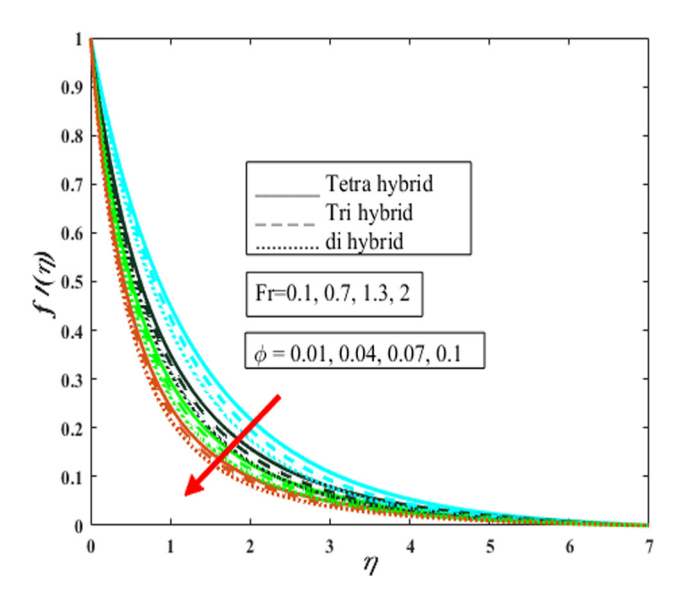


Figure 3: The procedure of the proposed model from numerical PDEs to numerical computations.



**Figure 4:** Impact of Forchheimer number Fr on the velocity field  $f'(\eta)$  by changing the volume fraction of the nanoparticles.

$$\varphi = y_6, \quad \varphi' = y_7,$$
 
$$\varphi'' = y_7' = -\left(\frac{\mathrm{Nt}}{\mathrm{Nb}}y_5' + \mathrm{Sc}y_1y_7 + \mathrm{Sc}\mathrm{Sr}y_5'\right)$$

with boundary conditions

$$\begin{split} \eta &= 0: y_1(\eta) = 0, \quad y_2(\eta) = 1, \quad y_4 = 1, y_6 = 1, \quad y_2(\eta) \\ &\to 0, \quad y_4(\eta) \to 0, \quad y_6(\eta) \to 0. \end{split}$$

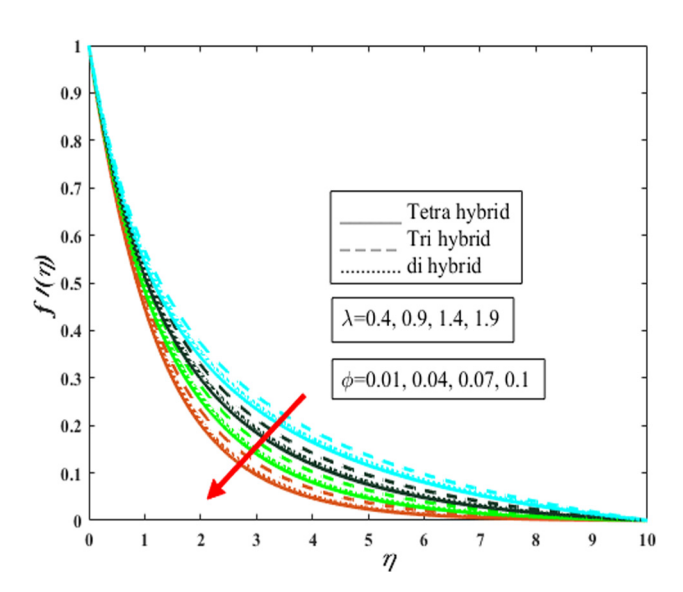


**Figure 5:** Influence of porosity  $\lambda$  on the velocity field  $f'(\eta)$  by changing the volume fraction of the nanoparticles.

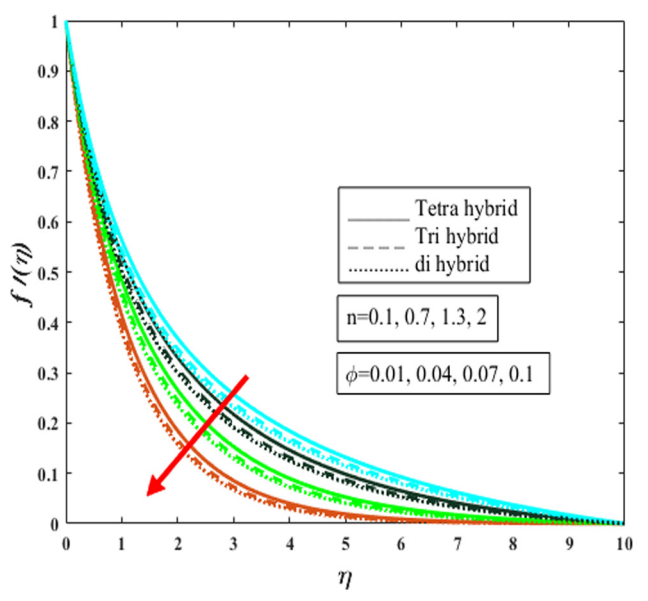


**Figure 6:** Effect of viscosity index n on the velocity field  $f'(\eta)$  by changing the volume fraction of the nanoparticles.

#### 6 Graphical results and discussions

#### 6.1 Velocity profile

Figures 4 and 5 are designed to check the Forchheimer number Fr and in addition to the porosity parameter  $\lambda$ on  $f'(\eta)$ . The viscidness of liquid increases by improving Fr providing resistance to liquid movement. It is observed that the fluid becomes more viscous with an increase in the fractional size of nanomolecules, which reduces the liquid speed shifting via an expandable medium and diminishes the rapidity outline  $f'(\eta)$ . Figure 4 illustrates the effect of the porosity factor  $\lambda$  on  $f'(\eta)$ . There is a relationship between the Darcian law and the porosity phenomena. The Darcian hypothesis states that the fluctuations in pressure and speed of a liquid are intimately connected. Since the Darcian body force acts in contrast to the porosity of the fluid-flowing medium, it slows down the movement of the fluid that it causes. The changes in pressure increase the density in addition to resistance. As shown in Figure 5, fluid faces difficulty in passing through the porous medium and moves closer to the vertical wall as a result. The implementation of n in relationship to  $f'(\eta)$  is shown in Figure 6. The symbol n represents the viscosity of the liquid, which conveys the aforementioned data. Viscosity has an upward trend for n > 1, remains constant for Newtonian fluids with n = 1, and decreases for n < 1. The viscosity of the fluid overcomes its inertia, leading to an increase in n and a decreases in  $f'(\eta)$ . The number proposed by Weissenberg is linked to the process of untwisting and is the duration required for a

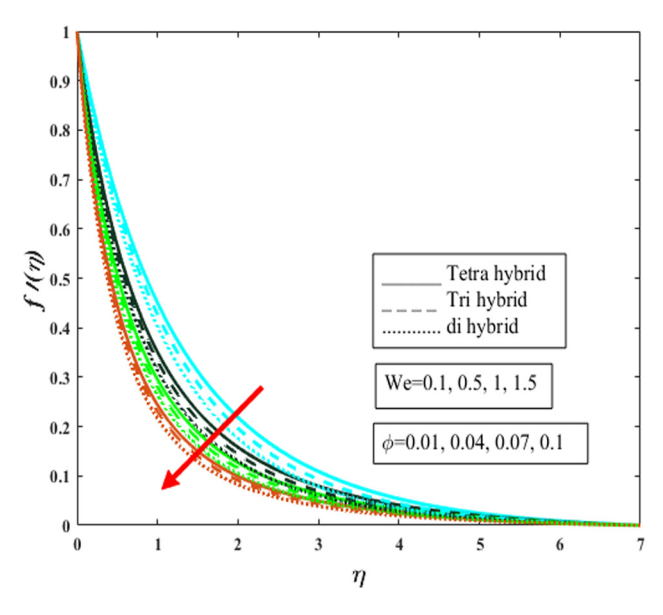


**Figure 7:** Impact of Weissenberg number We on the velocity field  $f'(\eta)$  by changing the volume fraction of the nanoparticles.

liquid to reach a state of relaxation. The viscosity decreases with increasing We and decreases the rate of flow. Consequently, this results in a decrease in the total speed. As shown in Figure 7, the decrease in shear viscosity that occurs with increasing We increases the average liquid rapidity.

#### 6.2 Temperature profile

Figures 8–13 illustrate the influence that a wide range of diverse factors has on the temperature  $\theta(\eta)$ .  $\theta(\eta)$  decreases

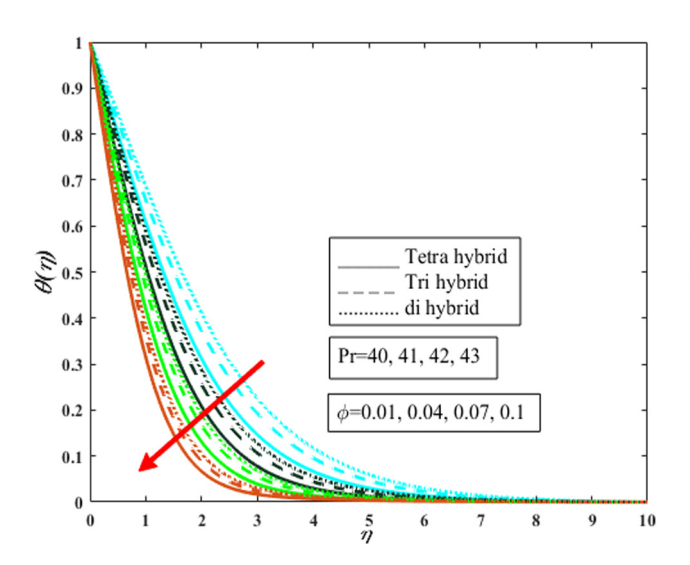


**Figure 8:** Effect of Prandtl number  $\Pr$  on the temperature field  $\theta(\eta)$  by changing the volume fraction of the nanoparticles.

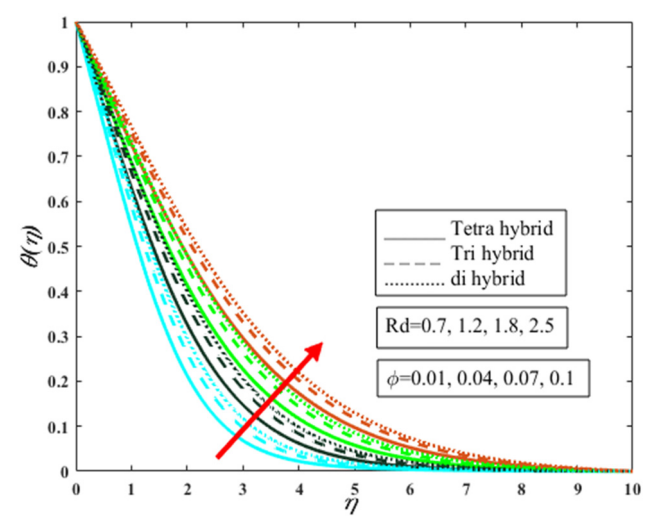


**Figure 9:** Effect of radiation number Rd on the temperature field  $\theta(\eta)$  by changing the volume fraction of the nanoparticles.

with an increase in Pr. Because of the increase in Pr, heat dissipates very rapidly, leading to a decrease in the amount of heat that is delivered and the temperature within the fluid. As displayed in Figure 8, the thermal boundary width increases as Rd increases, while it decreases with an increase in Pr. Figure 9 demonstrates the effect of the radiation parameter Rd on  $\theta(\eta)$ .

Thermal radiation flux is used in situations that need a significant temperature difference and has a wide range of applications in production, including nuclear reactors and combustible nuclear power plants, among others. The production of polymer substances, water treatment, and similar procedures are discussed. Increasing the value of

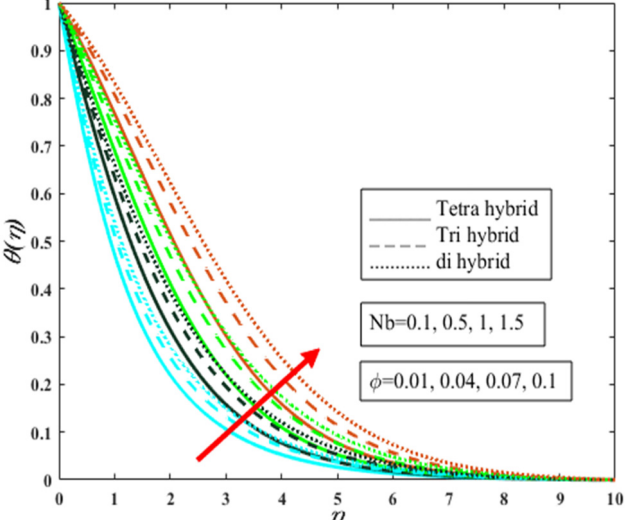


**Figure 10:** Effect of Brownian diffusion Nb on the temperature field  $\theta(\eta)$  by changing the volume fraction of the nanoparticles.

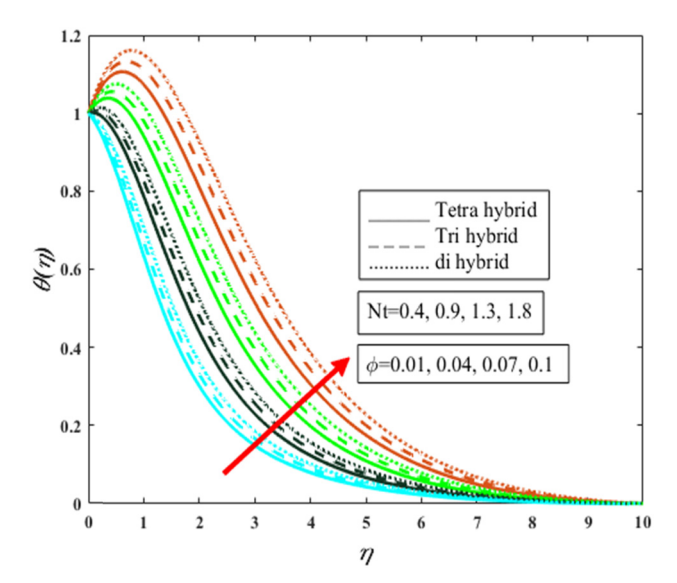


**Figure 11:** Effect of thermophoresis diffusion Nt on the temperature field  $\theta(\eta)$  by changing the volume fraction of the nanoparticles.

Rd leads to a higher degree of uncertainty in atomic collisions. The introduction of tetra nanocomponents to the traditional fluid enhances the Rd phenomena, resulting in an increase in  $\theta(\eta)$  and the thickening of a temperature boundary layer. This is due to the thickening of the temperature boundary layer. It is well-known that even an increase in the positive value of Nb has a multiplicative effect on the temperature of the fluid. The mobility of the particles in a fluid that exhibits a zigzag pattern is known as Brownian motion. It is not surprising that molecules crash into one other much more haphazardly and transfer some of their kinetic energy to each other. Such an increase in

temperature is caused by an interaction between two crucial factors of the Buongiorno nanofluid model (BNFM): the thermophoretic variable Nt and the Brownian diffusion parameter Nb. The enhancement of the thermophysical properties of the liquid caused by the incorporation of tetra nanomolecules in the conventional fluid is shown in Figure 10, and it leads to an increase in Nb as well as a greater quantity of heat transported and the temperature within the fluid. The effect of increasing Nt has on the temperature is shown in Figure 11. An increase in Nt generates a temperature difference, and this leads to an increase in the force (thermophoretic) that exists among nanoparticles. This force causes the heating up of more liquid, which in turn increases the temperature. It has been noticed that this force is greater when tetra-hybrid nanomolecules are incorporated into the standard liquid. The increased delivery of heat by nanofluid is due to an increase in Nt, which in turn increases  $\theta(\eta)$ . Figure 12 shows the results of the Dufour effect, abbreviated as Df, on the temperature field. It was noticed that the value of  $\theta(\eta)$  increases when there is a minuscule modification made to Df. Either the Dufour phenomena or the diffusion thermo effect may be used to refer to the process of heat transfer that occurs as a direct consequence of an isothermal chemical potential gradient. The transmission of heat is what sets the Dufour effect apart from several other types of events. It is a representation of the heat transference that occurs because of the diffusion that takes place when conditions are isothermal. Because of the integration of tetra hybrid nanomolecules and Buongiorno nanofluid, the heat transference, measured in conditions of Df, increases. The rate of heat transition and the temperature of the fluid both increase because of an increase in the thickening of the

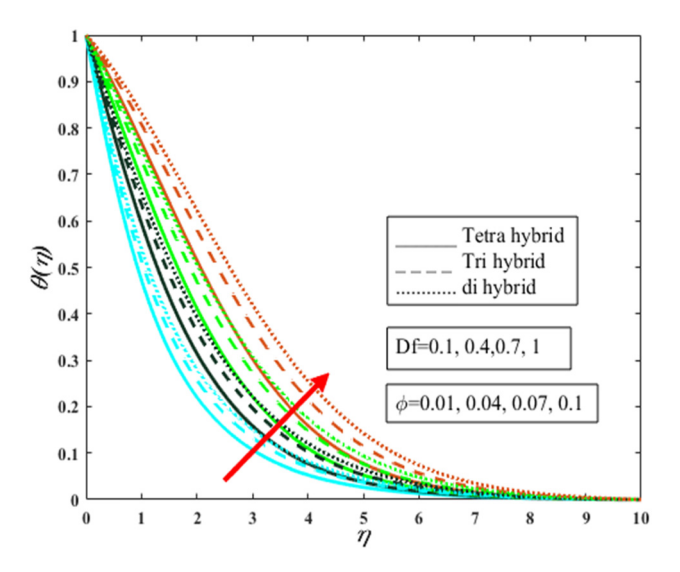


**Figure 12:** Effect of Dufour number Df on the temperature field  $\theta(\eta)$  by changing the volume fraction of the nanoparticles.

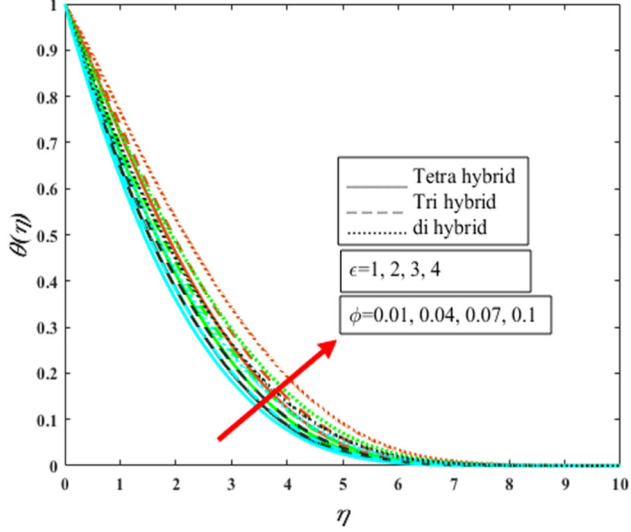


**Figure 13:** Effect of thermal conductivity  $\varepsilon$  on the temperature field  $\theta(\eta)$  by changing the volume fraction of the nanoparticles.

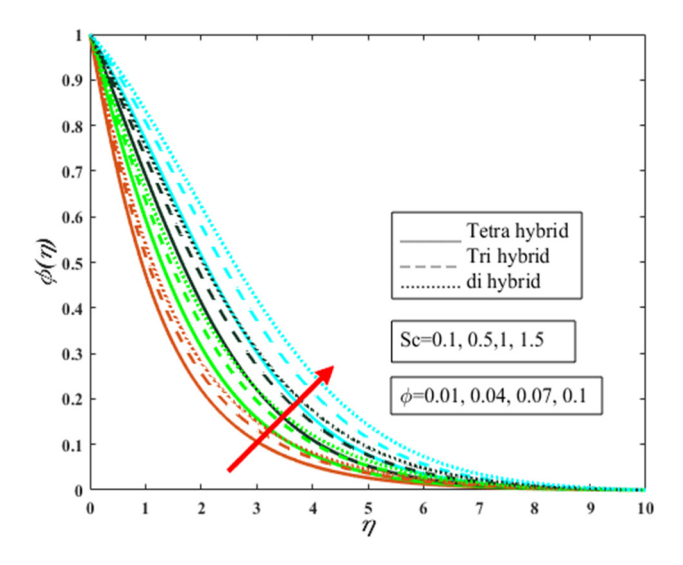


**Figure 14:** Effect of Schmidt number Sc on the concentration field  $\varphi(\eta)$  by changing the volume fraction of the nanoparticles.

temperature boundary layer. Thermal conductivity is used to describe the capacity of any substance to transfer heat. Particles collide more accidentally and transfer more heat in the presence of tetra hybrid nanoparticles, which increases  $\varepsilon$  and  $\theta(\eta)$ , as shown in Figure 13.

#### 6.3 Concentration profile

Figures 14 and 15 show the impact of Sc and Sr on  $\varphi(\eta)$ . A positive fluctuation in Sc and Soret effect Sr increases the concentration of the liquid. By increasing Sc and Sr,

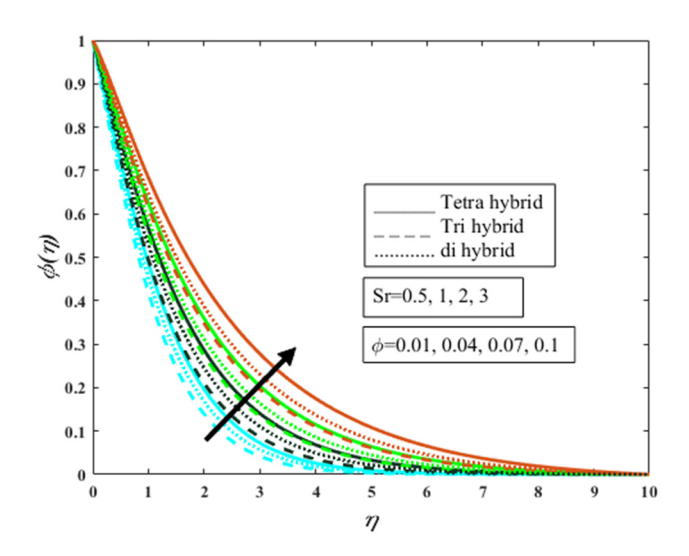


**Figure 15:** Behavior of Soret number  ${\rm Sr}$  on the concentration field  $\varphi(\eta)$  by changing the volume fraction of the nanoparticles.

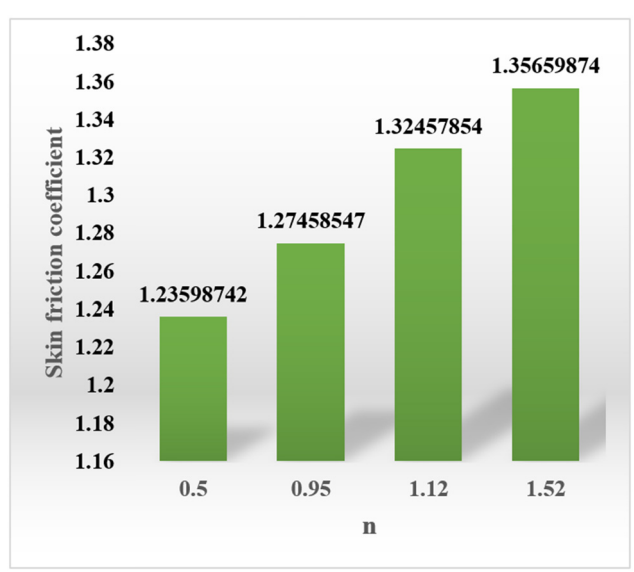


**Figure 16:** Effect of power law index *n* on the frictional force.

the density of the boundary layer increases. Sc is the ratio of momentum dispersion to mass dispersion. When the magnification in Sc is increased, the mass diffuses rapidly. Mass is closely related to the concentration, and a positive change in Sc increases  $\varphi(\eta)$ . It is well known that temperature and concentration have a significant relationship. Sr represents the proportion of temperature and concentration variation. When Sr is increased, the temperature gradient also increases, and there seems to be an increase in molecular dispersion. As a consequence, as Sr increases, the rate at which mass is transmitted increases.

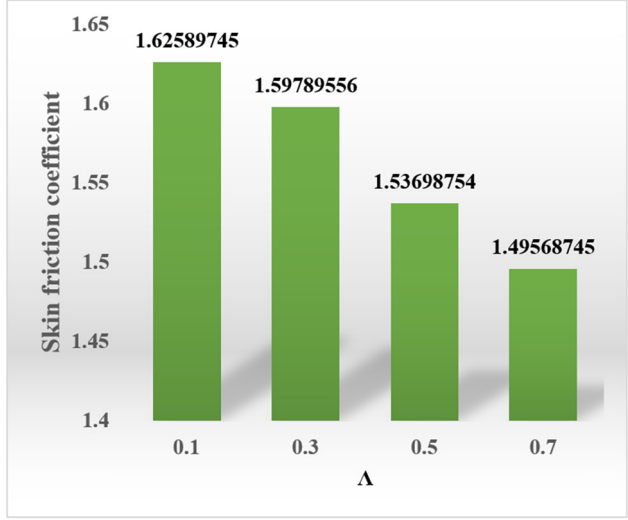


**Figure 17:** Effect of Maxwell fluid parameter  $\Lambda$  on the frictional force.

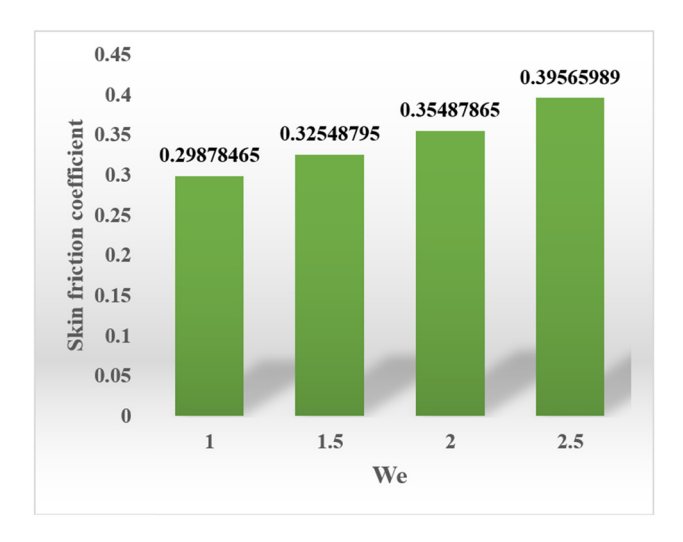
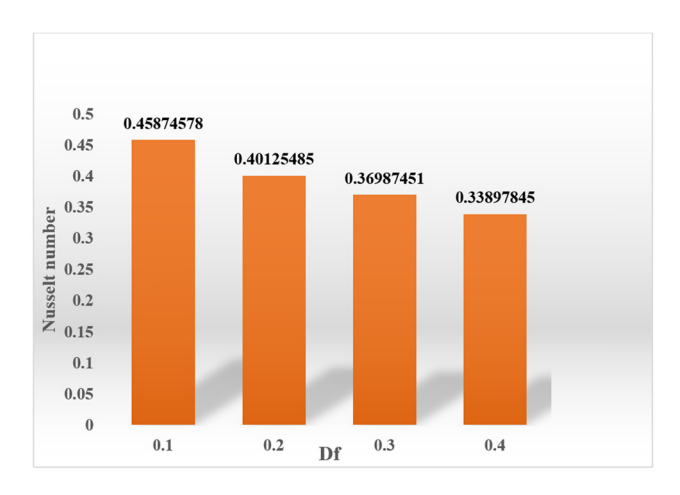


Figure 18: Effect of Weissenberg number We on the frictional force.

#### 6.4 Statistical analysis

The effectiveness of n and  $\Lambda$  on the drag coefficient is shown in Figures 16 and 17. The liquid velocity also decreases when the density increases in terms of n. Surface friction actually hinders the movement of liquids. A progressive effect in n increases the liquid viscosity, thereby decreasing the overall flow motion and increasing the frictional force. The findings of the Maxwell fluid variable on the frictional factor are shown in Figure 17. The rapidity of liquid flowing alongside the intermediate rapidity causes surface drag. The liquid velocity decreases because of an increase in  $\Lambda$ , which diminishes the wall frictional force. Physically, when a liquid's relaxation time increases, the drag friction effect and fluid velocity decrease. Figure 18 shows the effect of the Weissenberg number on the surface drag friction. The Weissenberg



**Figure 19:** Effect of Dufour number Df on the heat transfer Nusselt number.

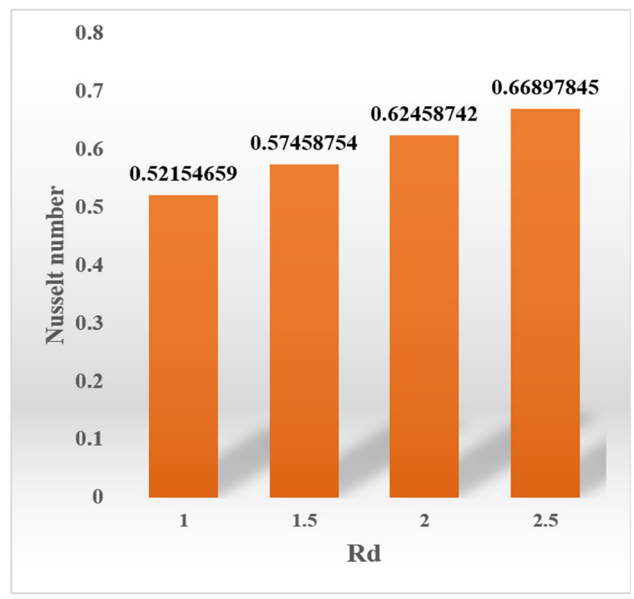


**Figure 20:** Investigation of thermal radiation Rd on the heat transfer Nusselt number.

number is related to how long a fluid must relax before it may resume its previous form. Fluid viscosity increases throughout that period, causing difficulty for the liquid to pass readily via the expanded plate. The friction that the liquid creates against the surface is known as drag friction. It is generally known that velocity decreases with an increase in We, which, on the other hand, increases drag friction, as shown in Figure 19. A crucial parameter increasing the rate of heat transport is Df. The Dufour quantity is favored by

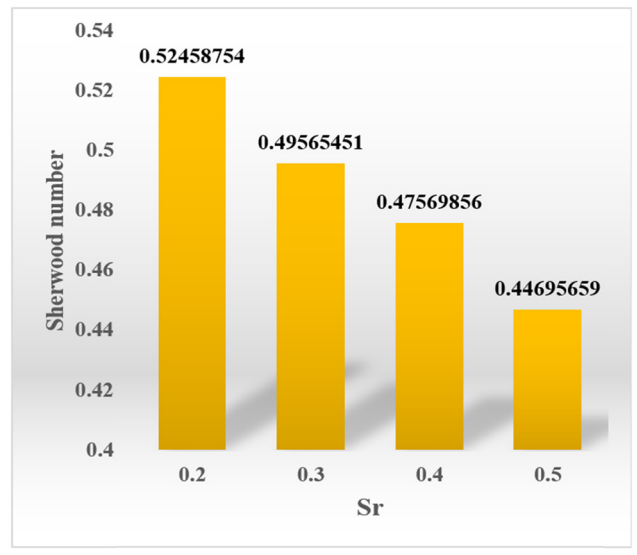


**Figure 21:** Impact of Soret number Sr on the concentration transport Sherwood number.

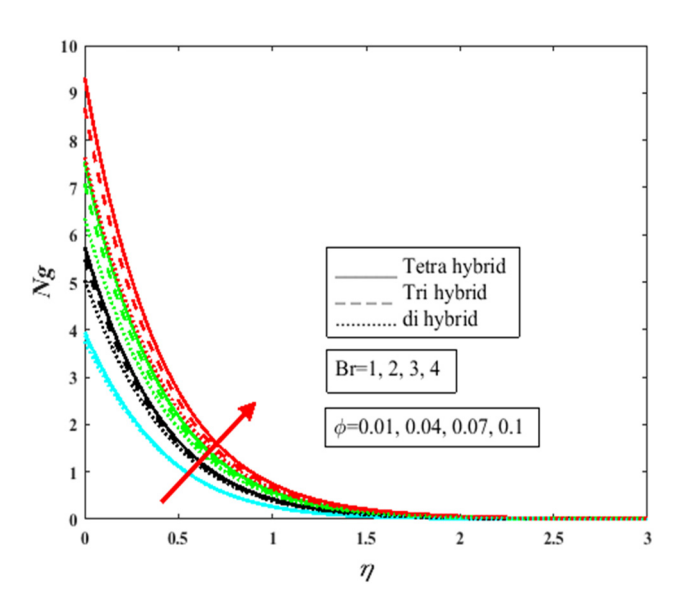


**Figure 22:** Impact of Brinkman number Br on the entropy generation Ng by changing the volume fraction of the nanoparticles.

temperature fluctuation, which magnifies the fluid's internal temperature. For Df, the use of Buongiorno tetra hybrid nanoparticles increases the fluid temperature and the velocity of heat transfer, which increases the Nusselt number, as illustrated in Figure 19. The introduction of nanomolecules in the standard liquid significantly elaborates the Rd behavior and Nusselt number, as shown in Figure 20, whereas incremental changes in Rd cause the fluid temperature to increase thermal conductivity. Figure 21 shows the impact of Sr on the Sherwood number. With an increase in Sr, fluid's mass transport and Sherwood number are decreased.

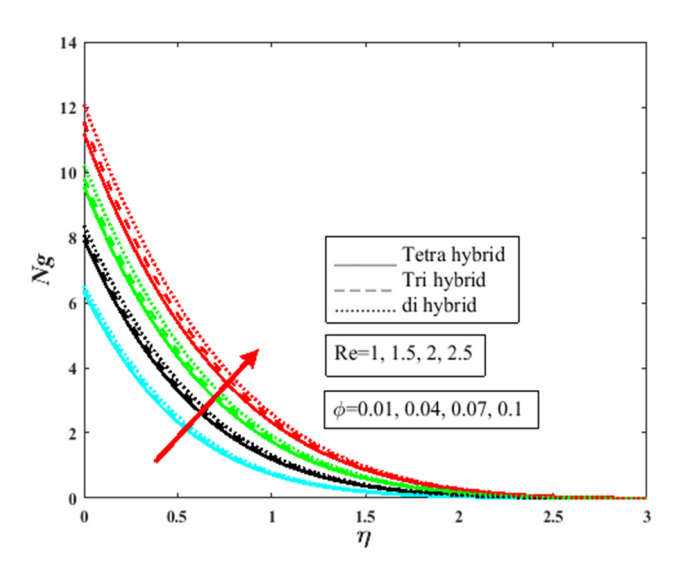


**Figure 23:** Impact of Reynolds number Re on the entropy generation Ng by changing the volume fraction of the nanoparticles.

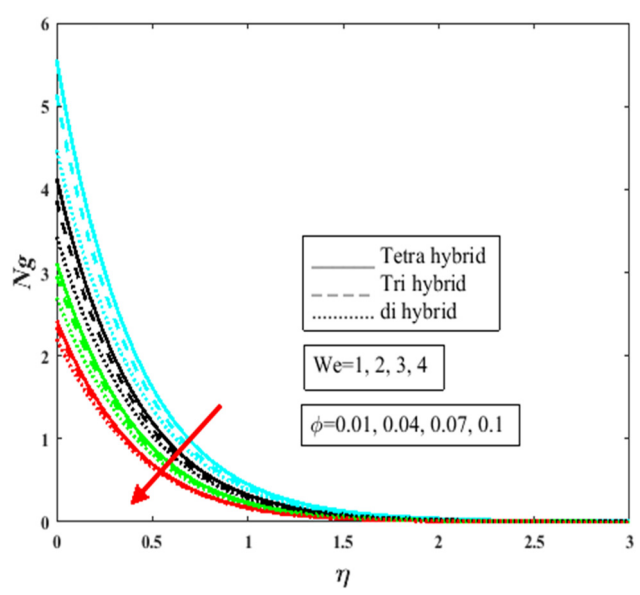


**Figure 24:** Impact of Weissenberg number We on the entropy generation Ng by changing the volume fraction of the nanoparticles.

#### 6.5 Entropy generation analysis

Figures 22 and 23 show the effects of Br and Re on the entropy generation Ng. When Br is increased, the physical characteristics change in such a manner that the conducting occurrence of heat that is formed because of viscous dissipation decreases. This phenomenon arises due to the fact that the rate at which heat is conducted increases proportionally with the temperature of the system. This phenomenon occurs due to an increase in the rate of heat conductance as the temperature of the

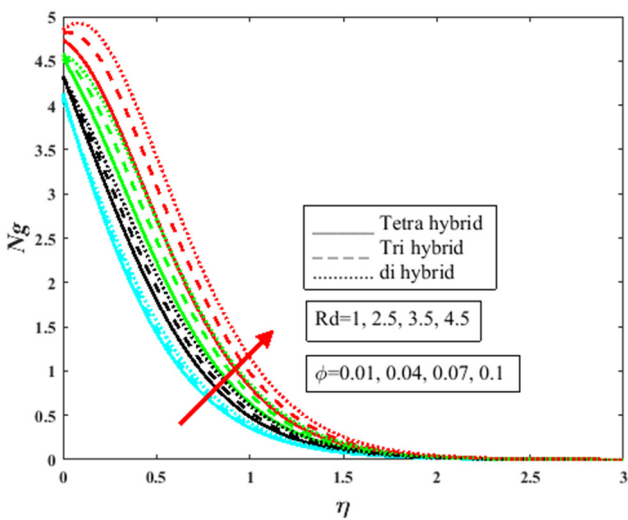


**Figure 25:** Impact of radiation Rd on the entropy generation Ng by changing the volume fraction of the nanoparticles.

system increases. Consequently, the pace at which entropy is formed increases as a direct effect of this. The change from laminar to turbulent behavior of the fluid that occurs because of an increase in Re is caused by this change. This is because the process of heat dissipation is exacerbated by increasing Re. which in turn emphasizes Ng. Figures 24 and 25 illustrate the entropy-creating process known as Ng, which occurs due to a progressive variation in both We and Rd. This is the major focus of interest that is spent on this process. The relaxation time of fluid increases with an increase in the We number, which provides the resistance to the flow of fluid, increases temperature on the other side, and decreases the Ng field. This obstruction to the flow of liquid is caused by an increase in the temperature. With an increase in Rd, molecules collide more often, absorbing more heat and sharing more KE. This extensive heat is sent to the liquid, which develops the overall entropy of the liquid and Ng. The molecules also share more KE with each other. An incremental change in the concentration diffusion L is found to result in faster diffusion of the mass, which was observed to occur as a consequence of the change. Molecules moved from a location that was hotter to a cooler region, which caused an imbalance in the concentration equilibrium and increased the overall entropy Ng of the system, as illustrated in Figure 26. The influence that Br and Re have on the Bejan number is shown in Figures 27 and 28. Both the generation of entropy and the qualities possessed are in direct opposition to one another. Whenever there is a positive variation in Br and Re, there is an accompanying increase in Ng, while there is a decrease in Be.

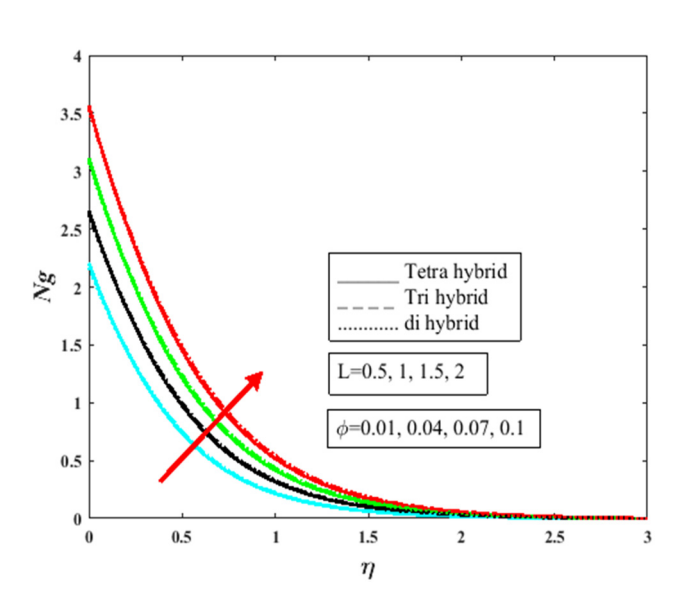


**Figure 26:** Impact of diffusion concentration L on the entropy generation Ng by changing the volume fraction of the nanoparticles.

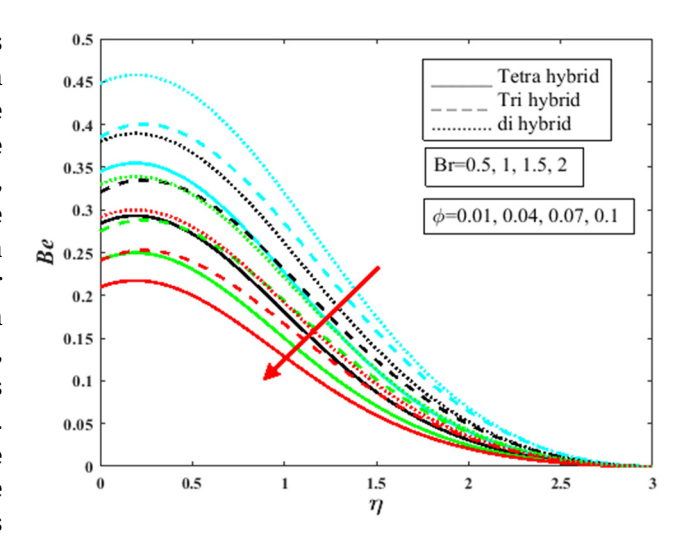


**Figure 27:** Impact of Brinkman number Br on Bejan number Be by changing the volume fraction of the nanoparticles.

## 7 An examination in the tabulated form of results acquired numerically

### 7.1 Effect of a variety of characteristics on the frictional force factor of the surface

Table 3 shows the effect of a wide diversity of influences on the drag coefficient. It is well known that drag frictions are forces that operate in the opposing direction of the material upon which the liquid is moving. A decrease in velocity as well as an increase in the drag friction are both found to result

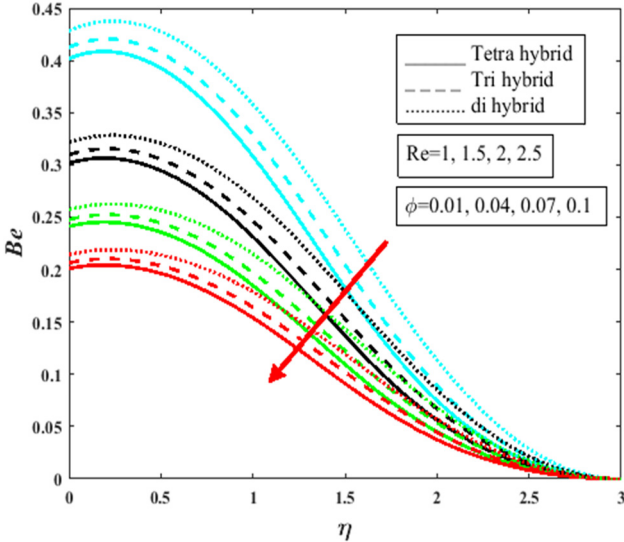


**Figure 28:** Impact of Reynolds's number Re on the Bejan number Be by changing the volume fraction of the nanoparticles.

6 — Tanveer Sajid et al. DE GRUYTER

Table 3: Influence of a variety of elements on the frictional force factor

n	Fr	λ	We	Λ	$C_{\mathbf{f}} \operatorname{Re}_{X}^{\frac{1}{2}}$
0.5	0.3	0.3	0.1	0.1	1.7321
1.2					1.3015
1.6					1.1278
	0.5				1.6345
	0.7				1.7214
	0.9				1.8510
		0.5			1.4143
		0.7			1.6015
		0.8			1.8231
			0.5		1.2176
			1		1.1015
			1.5		0.6312
				0.3	1.7213
				0.5	1.7487
				0.7	1.7854

from a significant change in Fr, We,  $\lambda$ , and  $\Lambda$ . It has been noticed that an increase in these factors causes resistance to the movement of liquid and decreases the velocity. It was found that increasing the viscous parameters n decreases the drag friction.

### 7.2 Effect of different factors on the Nusselt number

Table 4 displays the effects of various factors on the heat transportation phenomenon. The Nusselt number actually represents the temperature difference at the plate with the ratio of convection heat transference to conducting heat transport. A temperature change strengthens with an increase

**Table 5:** Influence of different dimensionless parameters on the Nusselt number by increasing the amount of nanoparticles

$\epsilon$	Nb	Nt	Rd	Di hybrid $\phi_{1+}\phi_2$	Tri hybrid $\phi_{1+}\phi_2+\phi_3$	Tetra hybrid $\phi_{1+}\phi_2 + \phi_3 + \phi_4$
0.5	0.5	0.5	0.5	2.2312	2.6213	2.9012
1				2.6145	2.9019	3.3121
1.5				2.8151	3.1214	3.5317
	1			2.4212	2.5116	2.7521
	1.5			2.6101	2.7368	2.9291
	2			2.8351	2.8481	3.4152
		1		2.1234	1.6241	1.4765
		1.5		1.8785	1.4413	1.3837
		2		1.7015	1.2147	1.2612
			1	2.8121	3.1209	3.8123
			1.5	3.1013	3.4561	4.1243
			2	3.4345	3.7215	4.3316

**Table 4:** Influence of different dimensionless parameters on the Nusselt number

Df	Rd	Nt	Nb	$\epsilon$	$Nu_x Re_x^{\frac{1}{2}}$
0.5	0.1	0.3	0.3	0.5	2.3954
0.1					2.5218
1.5					2.7115
2					2.9763
	0.4				2.6215
	0.7				2.8312
	1.0				3.1102
		0.6			2.5210
		0.9			2.3016
		1.2			2.2015
			0.6		2.7156
			0.9		3.2015
			1.2		3.5781
				1.0	3.1218
				1.5	3.4032
				2.0	3.6217

in Dufour number Df, radiative parameter Rd, Brownian diffusion Nb, and thermal conductivity  $\varepsilon$ , and decreases with an increase in the thermophoresis effect Nt.

## 7.3 Impact of parameters on the heat transportation phenomenon for di hybrid, ternary hybrid, and tetra hybrid nanoparticles

Table 5 shows the effect of  $\varepsilon$ , Nb, Nt, and Rd on heat transportation rates for di hybrid, tri hybrid, and tetra hybridity nanomolecules. It is well known that the inclusion of tetra nanomolecules increases the thermal conductance of the liquid and Nusselt number. It is observed that increases in  $\varepsilon$ , Nb, and Rd deliver more heat, and this heat generation is more dominant in the order tetra hybrid > ternary hybrid > dihybrid. It is reflected that the thermophoresis variable Nt decreases the heat transmission rate in the order di hybrid > tri hybrid > tetra hybrid, as shown in Table 5.

**Table 6:** Analysis of the achieved results regarding the surface frictional force factor

Parameter	Skin friction			
M	Khan <i>et al.</i> [54]	Existing findings		
0.1	1.0000	1.0000005		
0.5	1.1181	1.1181052		
1.0	1.4141	1.4142081		

0.0028

0.0013

0.6762

0.3540

1

1.5

0.5

0.5

-0.1101

-0.6853

Λ We  $Cf_x$  $b_1$  $\boldsymbol{b}_2$  $\boldsymbol{b}_3$  $b_4$  $\boldsymbol{b}_5$  $\varepsilon_1$ 0.1 1 0.5461 -0.2001 1.2642 0.0270 -0.4140 0.0612 0.0037 0.1 15 0.3412 -0.16211.6753 0.0212 -0.6126 0.0070 0.0015

0.1876

0.1213

1.3801

1.1739

**Table 7:** Optimal error calculation utilizing statistical quadratic regression analysis for surface drag by augmenting  $\Lambda$  and We

Table 8: Calculation of or	ptimal error for heat transition b	v improving $arepsilon$ and Rd in the case of $\mathfrak a$	uadratic regression analysis
Tubic of calculation of of	painal cirol for fieue d'alibidon a	improving a una Ra in the case of q	addiddic regression analysis

-0.7682

-0.4307

ε	Rd	$Nu_x$	$c_1$	$c_2$	$c_3$	$c_4$	<b>c</b> <sub>5</sub>	$oldsymbol{arepsilon}_2$
0.5	0.6	2.5360	0.0321	-0.0234	-0.0315	0.0245	0.1240	0.0152
0.5	1	2.5372	0.0035	-0.0439	-0.0011	0.0424	0.1763	0.0135
1.5	0.6	2.5456	0.0216	-0.0870	0.0012	0.3120	0.1854	0.0215
1.5	1	2.5481	0.0042	-0.0862	0.0215	0.2152	0.1801	0.0210

#### 8 Validation in the obtained results

0.8431

0.8156

Table 6 shows the analysis results caused by a positive variation in the inclined magnetic field M in the case of the drag coefficient. The findings obtained are more dependable and genuine in comparison to the ones produced by Khan et al. [30].

#### 9 Quadratic regression analysis for frictional factor and Nusselt number

The values of all the other distinguishable indicators are held constant throughout the procedure for carrying out a regression analysis. Throughout the cases of Cf<sub>x</sub> and Nu<sub>x</sub>, individual numerical characteristics are separated into 110 diverse sorts, allowing  $\Lambda$  and We amount for the drag coefficient as well as  $\varepsilon$  and Rd throughout the heat transition rate. All the remaining components range between 0.05 and 0.5 and between 0.05 and 0.20. The mathematical formulas representing a quadratic regression framework are as follows:

$$Cf_{qre} = Cf_x + b_1\Lambda + b_2We + b_3\Lambda^2 + b_4We^2 + b_5\Lambda We$$
, (25)

$$Nu_{qre} = Nu_x + c_1\varepsilon + c_2Rd + c_3\varepsilon^2 + c_4Rd^2 + c_5\varepsilon Rd.$$
 (26)

Here,  $b_1$ ,  $b_2$ ,  $b_3$ ,  $b_4$ ,  $b_5$ ,  $c_1$ ,  $c_2$ ,  $c_3$ ,  $c_4$ ,  $c_5$  are approximated values of drag coefficients and heat transport numerically achieved by regression analysis shown in Tables 7 and 8. Error computations in terms of  $Cf_x$  and  $Nu_x$  are achieved using  $\varepsilon_c = \frac{|Cf_{qre} - Cf_x|}{Cf_x}$  and  $\varepsilon_n = \frac{|Nu_{qre} - Nu_x|}{Nu_x}$ . Table 7 shows that the error becomes smaller by increasing n by taking We fixed

at  $\Lambda = 0.1$  and  $\Lambda = 0.5$ . According to Table 8, the error in terms of heat transition decreases by increasing  $\varepsilon$  and Rd.

#### 10 Conclusions

The purpose of this work is to explore the influence that a Buongiorno tetra hybrid nanofluid (BTHNF) model has on a Maxwell-cross liquid that is embedded with the Soret and Dufour effects and therefore is flowing while being exposed to an extendable surface. The conclusions are as follows:

- · Fluid thickness increases as a result of increases in the viscosity index n, the Weissenberg number We, and the Maxwell fluid parameter, all of which contribute to a reduction in the velocity field.
- · The rate on which heat is delivered increases as a consequence of a little modification to Rd, Df, and the thermal conductivity, which in turn increases the heat transport rate.
- · A decrease in fluid velocity results from even a little change in  $\lambda$  and Fr.
- The addition of tetra hybrid nanoparticles (THNF) to the foundation liquid causes an improvement in the heat capacity of the liquid. This, in turn, indicates a boost in the Nusselt numbers.
- In comparison to standard THNF, the BTHNF generates a greater amount of heat.
- Changing Rd while maintaining a constant value for  $\varepsilon$ results in a diminishing error in terms of the heat transfer rate. Similarly, changing We while maintaining a constant value for the Maxwell fluid parameter

results in a diminishing error in terms of the drag coefficient.

- Because of the increase in Br, Re, and Rd, there is a corresponding increase in the system's entropy.
- The Bejan number decreases as a consequence of the increasing effect that Br and Re have.
- Nanofluids with different effects like thermal radiation and thermal conductivity can be used as promising working fluids in different real-world industrial thermal energy systems, including heat exchangers, heat pipes, nuclear reactors, electronic cooling systems, and automobile radiators.
- This novel BTHNF model has been implemented in the case of fluid flow over various geometries like cone, wedge, cylinder, and Riga plates. Various nanofluid models like Maxwell, Hamilton-Crosser, Tiwari and Das, Yamada, and Ota nanofluid models have been modified in a similar fashion into ternary hybrid and tetra hybrid cases in order to achieve more heat.

**Acknowledgments:** The authors extend their appreciation to the Deanship of Scientific Research at King Khalid University for funding this work through a small group Research Project under grant number RGP.1/97/44.

**Funding information:** The authors extend their appreciation to the Deanship of Scientific Research at King Khalid University for funding this work through small group Research Project under grant number RGP.1/97/44.

**Author contributions:** Conceptualization: Wasim Jamshed; formal analysis: Tanveer Sajid; investigation: Wasim Jamshed; methodology: Mohamed R. Eid; software: Tanveer Sajid; regraphical representation and analysis of data: Salem Algarni; writing – original draft: Tanveer Sajid, Wasim Jamshed, and Mohamed R. Eid; writing – review editing: Talal Alqahtani; numerical process breakdown: Hijaz Ahmad; re-modeling design: Kashif Irshad; re-Validation: Ayesha Amjad. All authors have accepted responsibility for the entire content of this manuscript and approved its submission.

**Conflict of interest:** The authors state no conflict of interest.

#### References

[1] Megahed AM, Abbas W. Non-Newtonian Cross fluid flow through a porous medium with regard to the effect of chemical reaction and thermal stratification phenomenon. Case Stud Therm Eng. 2022;29:101715.

- [2] Hauswirth SC, Bowers CA, Fowler CP, Schultz PB, Hauswirth AD, Weigand T, et al. Modeling cross model non-Newtonian fluid flow in porous media. J Contam Hydrol. 2020;235:103708.
- [3] Patel HR. Cross diffusion and heat generation effects on mixed convection stagnation point MHD Carreau fluid flow in a porous medium. Int J Ambient Energy. 2021;43(1):1–16. doi: 10.1080/ 01430750.2021.1931960.
- [4] Shaw S, Samantaray SS, Misra A, Nayak MK, Makinde OD. Hydromagnetic flow and thermal interpretations of Cross hybrid nanofluid influenced by linear, non-linear and quadratic thermal radiations for any Prandtl number. Int Commun Heat Mass Transf. 2022;130:105816.
- [5] Sahu SK, Shaw S, Thatoi DN, Nayak MK. A thermal management of Darcy-Forchheimer SWCNT–MWCNT Cross hybrid nanofluid flow due to vertical stretched cylinder with and without inertia effects. Waves in Random and Complex Media; 2022. doi: 10.1080/ 17455030.2022.2088889. (Article in press).
- [6] Ramzan M, Shamshad U, Rehman S, Junaid MS, Saeed A, Kumam P. Analytical simulation of hall current and Cattaneo-Christov heat flux in cross-hybrid nanofluid with autocatalytic chemical reaction: An engineering application of engine oil. Arab J Sci Eng. 2023;48:3797–817.
- [7] Reddy VRM, Reddy MG, Dinesh PA, Sandeep N. Enhanced heat transfer efficiency of PTSC using hydromagnetic cross nanofluid: A hydrogen energy application. Int J Hydrog Energy. 2022;47:20254–64.
- [8] Ali M, Shahzad M, Sultan F, Khan WA. Numerical analysis of chemical reaction and non-linear radiation for magneto-cross nanofluid over a stretching cylinder. Appl Nanosci. 2020;10:3259–67.
- [9] Azam M, Shakoor A, Rasool HF, Khan M. Numerical simulation for solar energy aspects on unsteady convective flow of MHD Cross nanofluid: A revised approach. Int J Heat Mass Transf. 2019;131:495–505.
- [10] Asghar A, Lund LA, Shah Z, Vrinceanu N, Deebani W, Shutaywi M. Effect of thermal radiation on three-dimensional magnetized rotating flow of a hybrid nanofluid. Nanomaterial's. 2022;12:1566.
- [11] Khan U, Kumar RN, Zaib A, Prasannakumara BC, Ishak A, Galal AM, et al. Time-dependent flow of water-based ternary hybrid nanoparticles over a radially contracting/expanding and rotating permeable stretching sphere. Therm Sci Eng Prog. 2022;36:101521.
- [12] Algehyne EA, El-Zahar ER, Sohail M, Nazir U, AL-bonsrulah HAZ, Veeman D, et al. Thermal improvement in pseudoplastic material using ternary hybrid nanoparticles via non-Fourier's law over porous heated surface. Energies. 2021;14:8115.
- [13] Rasool G, Xinhua W, Lund LA, Yashkun U, Wakif A, Asghar A. Dual solutions of unsteady flow of copper-alumina/water based hybrid nanofluid with acute magnetic force and slip condition. Heliyon. 2023;9:e22737.
- [14] Hou E, Wang F, Nazir U, Sohail M, Jabbar N, Thounthong P. Dynamics of tri-hybrid nanoparticles in the rheology of pseudoplastic liquid with dufour and soret effects. Micromachines. 2022;13:201.
- [15] Prakasha DG, Sudharani MVVNL, Ganesh Kumar K, Chamkha AJ. Comparative study of hybrid (graphene/magnesium oxide) and ternary hybrid (graphene/zirconium oxide/magnesium oxide) nanomaterials over a moving plate. Int Commun Heat Mass Transf. 2023;140:106557.
- [16] Sarada K, Gamaoun F, Abdulrahman A, Paramesh SO, Kumar R, Prasanna GD, et al. Impact of exponential form of internal heat

- generation on water-based ternary hybrid nanofluid flow by capitalizing non-Fourier heat flux model. Case Stud Therm Eng. 2022;38:102332.
- [17] Shamshuddin MD, Akkurt N, Saeed A, Kumam P. Radiation mechanism on dissipative ternary hybrid nanoliquid flow through rotating disk encountered by Hall currents: HAM solution. Alex Eng J. 2023;65:543–59.
- [18] Sajid T, Ayub A, Shah SZH, Jamshed W, Eid MR, El Din ES, et al. Trace of chemical reactions accompanied with arrhenius energy on ternary hybridity nanofluid past a wedge. Symmetry. 2022:14:1850.
- [19] Roşca NC, Roşca AV, Aly EH, Pop I. Flow and heat transfer past a stretching/shrinking sheet using modified Buongiorno nanoliquid model. Mathematics. 2021;9:3047.
- [20] Puneeth V, Anandika R, Manjunatha S, Khan MI, Khan MI, Althobaiti A, et al. Implementation of modified Buongiorno's model for the investigation of chemically reacting rGO-Fe<sub>3</sub>O<sub>4</sub>-TiO<sub>2</sub>-H<sub>2</sub>O ternary nanofluid jet flow in the presence of bio-active mixers. Chem Phys Lett. 2022;786:139194.
- [21] Owhaib W, Al-Kouz W. Three-dimensional numerical analysis of flow and heat transfer of bi-directional stretched nanofluid film exposed to an exponential heat generation using modified Buongiorno model. Sci Rep. 2022;12:10060.
- [22] Ramesh GK, Madhukesh JK, Aly EH, Pop I. Modified Buongiorno's model for biomagnetic hybrid nanoliquid past a permeable moving thin needle. Int J Numer Methods Heat Fluid Flow. 2022;32:3551–78.
- [23] Ali B, Hussain S, Shafique M, Habib D, Rasool G. Analyzing the interaction of hybrid base liquid C<sub>2</sub>H<sub>6</sub>O<sub>2</sub>–H<sub>2</sub>O with hybrid nanomaterial Ag–MoS<sub>2</sub> for unsteady rotational flow referred to an elongated surface using modified Buongiorno's model: FEM simulation. Math Computers Simul. 2021;190:57–74.
- [24] Rana P, Gupta G. Numerical and sensitivity computations of threedimensional flow and heat transfer of nanoliquid over a wedge using modified Buongiorno model. Computers Math Appl. 2021;101:51–62.
- [25] Rana P, Mahanthesh B, Mackolil J, Al-Kouz W. Nanofluid flow past a vertical plate with nanoparticle aggregation kinematics, thermal slip and significant buoyancy force effects using modified Buongiorno model. Waves in Random and Complex Media; 2021. doi: 10.1080/17455030.2021.1977416. (Article in press).
- [26] Sabu AS, Areekara S, Mathew A. Regression analysis on MHD Darcy-Forchheimer hybrid nanoliquid flow over an elongated permeable sheet in a porous medium with hydrodynamic slip constraint: a realistic two-phase modified Buongiorno model. Waves in Random and Complex Media; 2022. p. 1–24. doi: 10.1080/ 17455030.2022.2086318. (Article in press).
- [27] Alblawi A, Malik MY, Nadeem S, Abbas N. Buongiorno's nanofluid model over a curved exponentially stretching surface. Processes. 2019;7:665.
- [28] Asogwa KK, Alsulami MD, Prasannakumara BC, Muhammad T. Double diffusive convection and cross diffusion effects on Casson fluid over a Lorentz force driven Riga plate in a porous medium with heat sink: An analytical approach. Int Commun Heat Mass Transf. 2022;131:105761.
- [29] Shoaib M, Rafia T, Raja MAZ, Khan WA, Waqas M. Further analysis of double-diffusive flow of nanofluid through a porous medium situated on an inclined plane: AI-based Levenberg–Marquardt scheme with backpropagated neural network. J Braz Soc Mech Sci Eng. 2022;44(6):227.

- [30] Yadav D, Kumar Awasthi M, Al-Siyabi M, Al-Nadhairi S, Al-Rahbi A, Al-Subhi M, et al. Double diffusive convective motion in a reactive porous medium layer saturated by a non-Newtonian Kuvshiniski fluid. Phys Fluids. 2022;34(2):024104.
- [31] Ramchandraiah C, Kishan N, Reddy GSK, Paidipati KK, Chesneau C. Double-diffusive convection in bidispersive porous medium with coriolis effect. Math Comput Appl. 2022;27:56.
- [32] Murray BT, Chen CF. Double-diffusive convection in a porous medium. J Fluid Mech. 1989;201:147–66.
- [33] Asghar A, Chandio AF, Shah Z, Vrinceanu N, Deebani W, Shutaywi M, et al. Magnetized mixed convection hybrid nanofluid with effect of heat generation/absorption and velocity slip condition. Heliyon. 2023;9:e13189.
- [34] Yogeesha KM, Megalamani SB, Gill HS, Umeshaiah M, Madhukesh JK. The physical impact of blowing, Soret and Dufour over an unsteady stretching surface immersed in a porous medium in the presence of ternary nanofluid. Heat Transf. 2022;51:6961–76.
- [35] Hafeez MB, Sumelka W, Nazir U, Ahmad H, Askar S. Mechanism of solute and thermal characteristics in a casson hybrid nanofluid based with ethylene glycol influenced by soret and dufour effects. Energies. 2021;14:6818.
- [36] Song Y-Q, Khan MI, Qayyum S, Gowda RP, Kumar RN, Prasannakumara B, et al. Physical impact of thermo-diffusion and diffusion-thermo on Marangoni convective flow of hybrid nanofluid (MnZiFe<sub>2</sub>O<sub>4</sub>–NiZnFe<sub>2</sub>O<sub>4</sub>–H<sub>2</sub>O) with non-linear heat source/sink and radiative heat flux. Mod Phys Lett B. 2021;35(22):2141006.
- [37] Dharmaiah G, Dinarvand S, Durgaprasad P, Noeiaghdam S. Arrhenius activation energy of tangent hyperbolic nanofluid over a cone with radiation absorption. Results Eng. 2022;16:100745.
- [38] Nasir S, Berrouk AS, Aamir A, Shah Z. Entropy optimization and heat flux analysis of Maxwell nanofluid configurated by an exponentially stretching surface with velocity slip. Sci Rep. 2023;13(1):2006.
- [39] Berrehal H, Dinarvand S, Khan I. Mass-based hybrid nanofluid model for entropy generation analysis of flow upon a convectivelywarmed moving wedge. Chin J Phys. 2022;77:2603–16.
- [40] Al Oweidi KF, Shahzad F, Jamshed W. Partial differential equations of entropy analysis on ternary hybridity nanofluid flow model via rotating disk with hall current and electromagnetic radiative influences. Sci Rep. 2022;12:20692.
- [41] Naz R, Tariq S, Sohail M, Shah Z. Investigation of entropy generation in stratified MHD Carreau nanofluid with gyrotactic microorganisms under Von Neumann similarity transformations. Eur Phys J Plus. 2020;135(2):178.
- [42] Dharmaiah G, Dinarvand S, Rama Prasad JL, Noeiaghdam S, Abdollahzadeh M. Non-homogeneous two-component Buongiorno model for nanofluid flow toward Howarth's wavy cylinder with activation energy. Results Eng. 2023;17:100879.
- [43] Falodun BO, Ige EO. Linear and quadratic multiple regressions analysis on magneto-thermal and chemical reactions on the Casson-Williamson nanofluids boundary layer flow under Soret-Dufour mechanism. Arab | Basic Appl Sci. 2022;29(1):269–86.
- [44] Sajid T, Jamshed W, Ibrahim RW, Eid MR, Abd-Elmonem A, Arshad M. Quadratic regression analysis for non-linear heat source/sink and mathematical Fourier heat law influences on Reiner-Philippoff hybrid nanofluid flow applying Galerkin finite element method. J Magn Magn Mater. 2023;568:170383.
- [45] Nandi S, Kumbhakar B, Seth GS. Quadratic regression analysis of unsteady MHD free convective and radiative–dissipative stagnation

- flow of hybrid nanofluid over an exponentially stretching surface under porous medium. Chin | Phys. 2022;77:2090–105.
- [46] El Din SM, Darvesh A, Ayub A. Quadratic multiple regression model and spectral relaxation approach for Carreau nanofluid inclined magnetized dipole along stagnation point geometry. Sci Rep. 2022;12:17337.
- [47] Raju CSK, Ahammad NA, Sajjan K, Shah NA, Yook S-J, Dinesh Kumar M. Non-linear movements of axisymmetric ternary hybrid nanofluids in a thermally radiated expanding or contracting permeable Darcy Walls with different shapes and densities: Simple linear regression. Int Commun Heat Mass Transf. 2022;135:106110.
- [48] Dinarvand S, Behrouz M, Ahmadi S, Ghasemi P, Noeiaghdam S, Gamiz UF. Mixed convection of thermomicropolar AgNPs-GrNPs nanofluid: An application of mass-based hybrid nanofluid model. Case Stud Therm Eng. 2023;49:103224.
- [49] Dinarvand S, Berrehal H, Tamim H, Sowmya G, Noeiaghdam S, Abdollahzadeh M. Squeezing flow of aqueous CNTs-Fe<sub>3</sub>O<sub>4</sub> hybrid nanofluid through mass-based approach: Effect of heat source/ sink, nanoparticle shape, and an oblique magnetic field. Results Eng. 2023;17:100976.

- [50] Dinarvand S, Berrehal H, Pop I, Chamkha AJ. Blood-based hybrid nanofluid flow through converging/diverging channel with multiple slips effect: a development of Jeffery-Hamel problem. Int J Numer Methods Heat Fluid Flow. 2023;33:1144–60.
- [51] Dinarvand S, Yousefi M, Chamkha A. Numerical simulation of unsteady flow toward a stretching/shrinking sheet in porous medium filled with a hybrid nanofluid. J Appl Comput Mech. 2022;8(1):11–20.
- [52] Lund LA, Asghar A, Rasool G, Yashkun U. Magnetized casson Sahybrid nanofluid flow over a permeable moving surface with thermal radiation and Joule heating effect. Case Stud Therm Eng. 2023;50:103510.
- [53] Asghar A, Vrinceanu N, Ying TY, Lund LA, Shah Z, Tirth V. Dual solutions of convective rotating flow of three-dimensional hybrid nanofluid across the linear stretching/shrinking sheet. Alex Eng J. 2023:75:297–312.
- [54] Khan M, Malik MY, Salahuddin T, Khan I. Numerical modeling of Carreau fluid due to variable thicked surface, Results in Physics. 2017;7: 2384–390.